



Molecular structure solvent-solute, electronic, topology and dynamics simulation studies on 2-[[1-(cyclopropyl methoxy)-4-hydroxy-2-oxoquinoline-3-carbonyl] amino] acetic acid- an effective CKD drug

P. Manikandan ^a, M. Kumar ^a, S. Chithra ^a, A. Jeelani ^a, Jamal M. Khaled ^b, Ghulam Abu-S ^c, S. Muthu ^{a,*}

^a Department of Physics, Aringar Anna Govt. Arts College, Cheyyar 604407, Tamil Nadu, India

^b Department of Botany and Microbiology, College of Science, King Saud University, P.O. Box 2455, Riyadh 11451, Saudi Arabia

^c Institute of Inorganic Chemistry, Karlsruhe Institute of Technology, Engesserstr 15, 76131 Karlsruhe, Germany

ARTICLE INFO

Keywords:

DFT
FTIR
NBO
HOMO-LUMO
Topological analysis

ABSTRACT

The current theoretical work analyzes the optimal structure and vibrational assignments of 2-[[1-(cyclopropyl methoxy)-4-hydroxy-2-oxoquinoline-3-carbonyl] amino] acetic acid (2C2O), examined theoretically through DFT method. PED values were calculated, and vibrational assignments have been determined. Studies employing FT-IR and FT-Raman methods were explored in both experimental and theoretical scenarios. By using Gaussian 09W, structural optimization, all bond parameters are examined. MEP differentiates nucleophilic and electrophilic sites and establishes a molecule's 3-dimensional charge distribution using gas and solvent phases. Global descriptors and band gap energies are provided using the Frontier Molecular Orbital(FMO) study. The electron delocalization resulting from hyperconjugation can be understood by using the NBO method. The TD-DFT technique and FUKUI model were utilized to stimulate the UV spectra of the title compound. FUKUI function was used to trace the area of reactive sites. Topological explorations were scrutinized using the Multiwave function. The title chemical exhibits a promising pharmacological profile. In this research, we assess its bioactivities and drug likeness. Molecular docking using Autodock technique reveals the compounds inhibiting effect on receptor. Analysis of the protein-ligand complexes stability was done using MD simulations.

1. Introduction

The development of important breakthroughs in the treatment of several fatal illness has been made possible by heterocyclic molecules [1]. Quinoline compounds have been frequently employed as a "parental" compounds to create and contribute molecules having an enormous assortment of Pharmacological behaviors, for instance anti-fungal, antileishmanial, anti-cancer, antiviral, anti-inflammatory, and anti-microbial activities [2–14]. Quinolone type medications are thought to be highly well tolerated, displaying just a small number of side effects when undergoing treatments [15]. The quinolone molecule is also the foundation of several potential anti-inflammatory and anti-cancer beneficial medicines, in contrast, quinolone derivatives offer a structure for industrial applications, such as OLED and solar cells, as

well as solvents for terpene and adhesive [16]. The creation of novel Quinoline underlying structure necessitates the significant investment in unification methods and structural layout due to the existence and significance of Quinoline a pharmacological substance in a variety of natural synthetic products. This is essential component of our investigation. In this study 2-[[1-(cyclopropylmethoxy)-4-hydroxy-2-oxoquinoline-3-carbonyl] amino] acetic acid (2C2O) is characterized. The drug used to treat with anemia corresponds to CKD [17].

The information of the title molecule(2C2O), which possesses chemical formula C₁₆H₁₆N₂O₆ and a molecular weight 332.2 g/mol, could be gathered from the drug bank. According to an analysis of the literature, on this molecule(2C2O), no calculations involving quantum chemicals have been performed so far. DFT is one of the effective approaches that has arisen in recent decades for the study of chemical

* Corresponding author.

E-mail address: mutgee@gmail.com (S. Muthu).

systems. Density Functional Theory (DFT) as well – established theoretical framework within the domain of quantum mechanics. It enables a thorough exploration of the electronic characteristics of intricate systems comprising a multitude of particles. This versatile approach encompasses wide range of entities, including condensed phases, molecules and atoms, with a primary emphasis on characterizing their ground state configurations. The principal objective of the current work is evaluating optimised compound structure, FMOs, UV exploration, FUKUI function, topological study and molecular docking interaction with various proteins.

2. Experimental details

The product 2-[[1-(cyclopropylmethoxy)-4-hydroxy-2-oxoquinoline-3-carbonyl] amino]acetic acid also known by the abbreviation 2C2O was purchased from a standard chemical company in its solid condition. FT-IR spectrum was acquired using an Alpha II Bruker FT-IR spectrometer, covering the range of 4000–400 cm⁻¹. And, the FT-Raman spectrum of 2C2O was obtained using MultiRAM Bruker FT-Raman spectrometer with 4000–400 cm⁻¹ ranges. These studies were made at JAMAL INSTRUMENTATION CENTRE (JAMIC), Tiruchirappalli, India.

3. Computational methods

The Gaussian09W [18] is used for the computational procedure and the high level basis set DFT - B3LYP / 6-311++G (d, p) is employed to find more efficient. The default convergence criteria were applied in all geometry optimizations. Using VEDA [19] program, the vibrational wavenumbers of 2C2O are estimated together with PED contribution. The investigation into the electronic properties of the aforementioned compound was carried out through methods of gas phase and solvent based assessments involving Aqueous, Dimethyl sulfoxide, ethyl alcohol

and methanol. Using IEFPCM model, analyses of HOMO - LUMO, UV-Vis and electrostatic potential was carried out in the gas and solvents above stated. In order to acquire insights into the molecular interactions among orbitals, NBO calculations were conducted. The same basis set was used for Mulliken charges, dual descriptor and fukui function calculations. Multiwave function [20] is utilized to determine topological parameters such as ELF, LOL and RDG. Application of the Autodock4.2.6 [21] software package has been made for molecular docking research.

4. Results and discussion

4.1. Geometry optimization

The Molecular structure of title compound 2C2O obtained using Chemcraft [22] visualization program and optimized using basis set of DFT / B3LYP / 6-311++G (d, p) method revealed in Fig. 1. Title compound contains Fifteen (Carbon – carbon) Bonds, Thirteen (Carbon – Hydrogen) Bonds, Four (Carbon – Nitrogen) Bonds, Six (Carbon – Oxygen) and Two (Oxygen – Hydrogen) Bonds and Single (O—N, N—H) bond lengths independently. The Large bonding length get it from (C23—C24) for 1.525 Å. And the minimum bond length discovers at (O5—H40) of 0.97 Å. The salient bond angle (maximum value) are detect theoretically in (C10—C24—O6) of 122.6° and the smallest bond angles are noted to 77.9° in C10—C11—H28 respectively. Table 1 presents the theoretical predictions for Bond angles and lengths.

4.2. Vibrational assignment

The impact of functional groups and their structural features and molecular confirmations has been explained in a significant manner by vibrational spectroscopy. The greatest number of observable functions in a non-linear molecule with (N) number of atom gets 3 N-6 for its

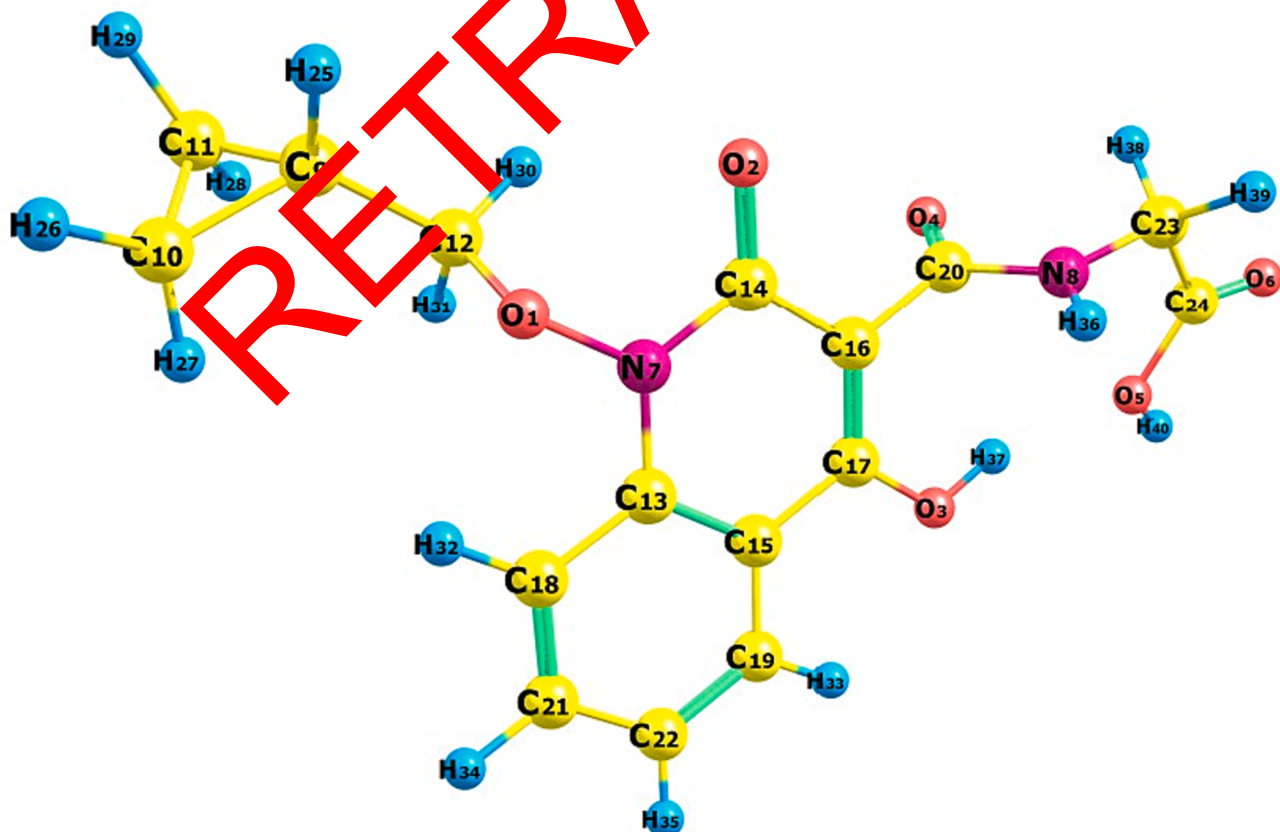


Fig. 1. Optimized molecular structure of 2C2O.

Table 1

Theoretical Bond lengths and Angles of the title compound 2C2O.

Bond length (Å)	DFT B3LYP/6-311++G(d,p)	Bond Angle (°)	DFT B3LYP/6-311++G(d,p)	Bond Angle (°)	DFT B3LYP/6-311++G(d,p)
O1—N7	1.384	N7—C1—C12	111.5	C11—C10—H26	118.5
O1—C12	1.46	C1—N7—C13	116.7	C11—C10—H27	117.7
O2—C14	1.22	C1—N7—C14	116.9	C10—C11—H28	117.9
O3—C17	1.351	C1—C12—C9	107	C10—C11—H29	118.6
O3—H37	0.972	C1—C12—H30	108.2	H26—C10—H27	114.4
O4—C20	1.216	C1—C12—H31	108.7	H28—C11—H29	114.2
O5—C24	1.364	C2—C14—N7	121.3	H30—C12—H31	109.9
O5—H40	0.97	C2—C14—C16	124.7	C15—C13—C18	119.8
O6—C24	1.2	C17—O3—H37	112.7	C13—C15—C17	118.2
N7—C13	1.385	O3—C17—C15	115	C13—C15—C19	119.3
N7—C14	1.407	O3—C17—C16	124.1	C13—C18—C21	119.6
N8—C20	1.373	O4—C20—N8	122.4	C13—C18—C32	119.1
N8—C23	1.442	O4—C20—C16	123.3	C14—C16—C17	122.3
N8—H36	1.008	C24—O5—H40	107.1	C14—C16—C20	117.4
C9—C10	1.509	O5—C24—O6	122.6	C17—C15—C19	122.5
C9—C11	1.511	O5—C24—C23	113.4	C15—C17—C16	120.9
C9—C12	1.497	O6—C24—C23	124	C15—C10—C22	120.7
C9—H25	1.084	C13—N7—C14	125.5	C15—C19—H3	118.4
C10—C11	1.507	N7—C13—C15	118.8	C17—C16—C20	120.3
C10—H26	1.083	N7—C13—C18	121.5	C2—C18—H32	121.2
C10—H27	1.084	N7—C14—C16	114	C18—C21—C22	121.1
C11—H28	1.084	C20—O8—C23	121.4	C18—C2—H3	119.1
C11—H29	1.083	C20—O8—H36	118.7	C2—C19—H3	120.9
C12—H30	1.091	N8—C20—C16	114.2	C19—C2—C21	119.6
C12—H31	1.096	C23—N8—H36	119.8	C19—C2—H35	120.2
C13—C15	1.415	N8—C23—C24	115.2	C22—C21—H34	119.8
C13—C18	1.405	N8—C23—H38	109	C1—C22—H36	120.2
C14—C16	1.456	N8—C23—H39	110.5	C24—C23—H38	106.5
C15—C17	1.444	C10—C9—C11	120.6	C24—C23—H39	107.4
C15—C19	1.406	C10—C9—C12	116.7	H38—C23—H39	107.5
C16—C17	1.367	C10—C9—H25	60.1		
C16—C20	1.505	C9—C10—C11	117.9		
C18—C21	1.385	C9—C10—H26	60		
C18—H32	1.08	C9—C10—H27	118.9		
C19—H22	1.383	C11—C9—C12	64.4		
C19—H33	1.082	C11—C9—H25	60		
C21—C22	1.402	C9—C11—C10	118		
C21—H34	1.084	C9—C11—H26	117.7		
C22—H35	1.083	C9—C11—H29	114		
C23—C24	1.525	C12—C9—H30	111.5		
C23—H38	1.092	C9—C12—C31	111.5		
C23—H39	1.091	C9—C12—H31			

Å: angstrom unit °: degree.

three degree of freedom in rotation and translation [23–25]. The title compound entails 40 atoms and 112 typical vibration modes. The frequencies attained from the calculations were adjusted wield a scaling factor 0.961 [26]. The individualistic vibrational assessment for the calculated wavenumbers, were generated based on the PED using VEDA4.

Fig. 2a and **Fig. 2b** illustrate a comparative analysis of theoretical and experimental FT – IR and FT – Raman spectra. **Table 2** gives the details of IR intensities and Raman Scattering and PED Assignments [27].

4.2.1. Oxygen-Hydrogen vibrations

O—H Stretching frequency values have been used for many years to test and quantify the strength of hydrogen bonds [28]. Typically, the foremost range for O—H stretching vibrations lies approximately within 3600–3400 cm⁻¹ [29] hydrogen bonds are the most vulnerable to these vibrations [30]. OH stretching vibrational modes was determining theoretically in 3606 cm⁻¹, 3540 cm⁻¹ and experimentally determined (FT-IR) at 3750 cm⁻¹. PED contribution is hundred percentages in 3606 cm⁻¹ and ninety-nine percentages in 3540 cm⁻¹. This indicates its a pure stretching modes.

4.2.2. Nitrogen – Hydrogen vibration

Vibrations related with the stretching of the N—H bonds are found amidst the range of 3300–3500 cm⁻¹ [31] N—H has a weaker advantage in forming a hydrogen bond its absorption is generally sharper. The precise location of absorption within this particular field is determined

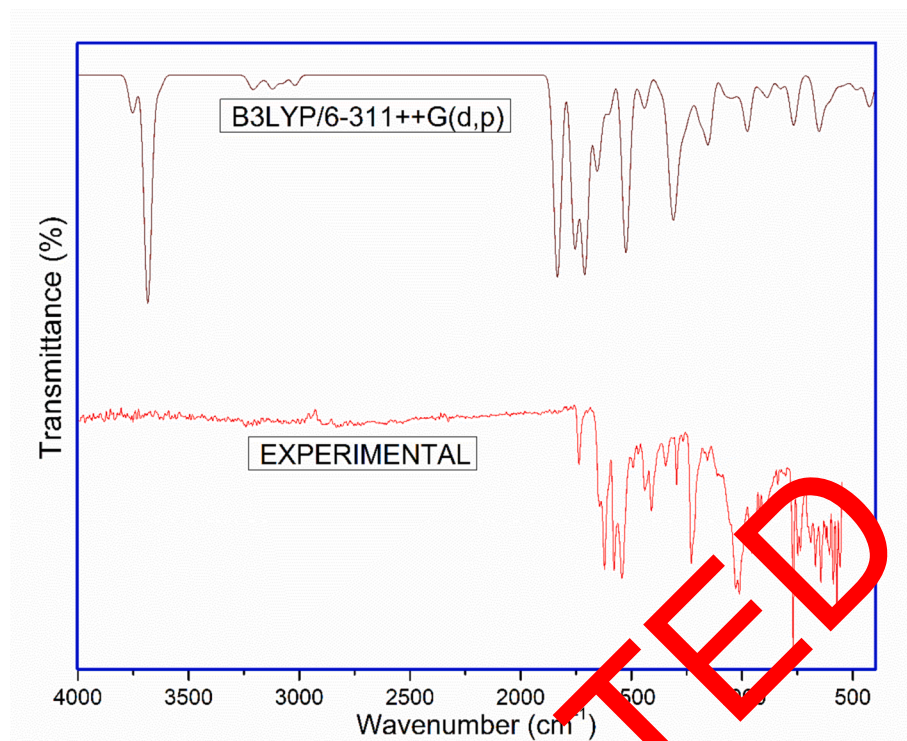
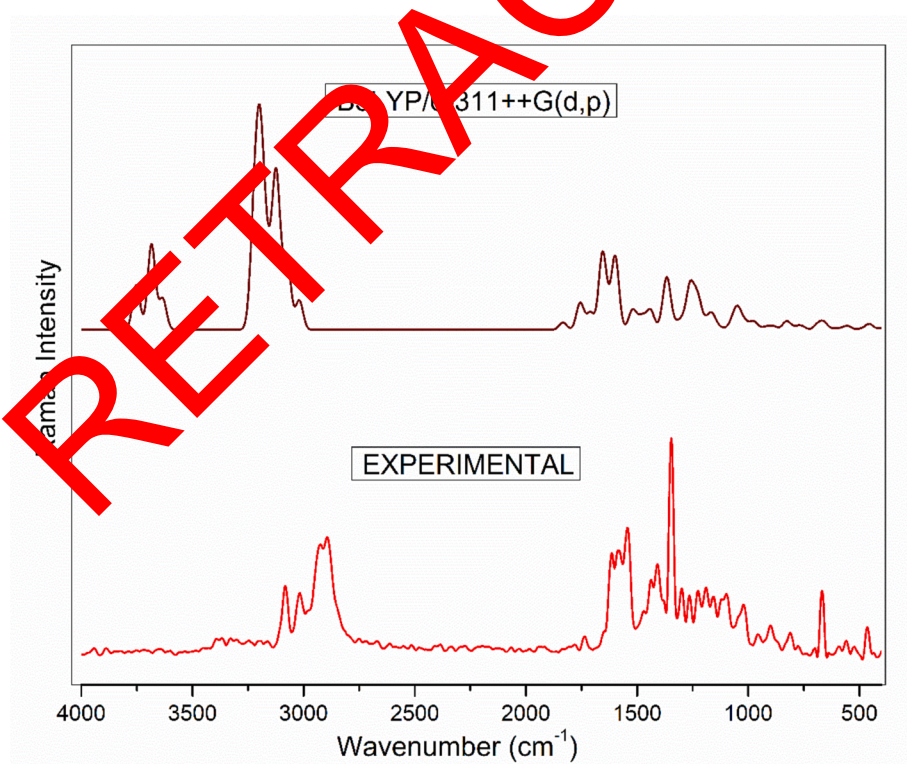
by strength like the hydrogen bonding, which is reflected by the chemical structure of compound or the solvents polarity [32]. Detection of N—H stretching vibration experimentally at 3240 cm⁻¹ in FT-IR and calculated 3492 cm⁻¹ in theoretically and its PED contribution is Hundred percentages.

4.2.3. Carbon – Hydrogen vibration

The arrangement reveals vibrations for stretching C—H occurrence within the 3200–3000 cm⁻¹ range [33,34]. Which is recognizable zone for CH stretching vibrations. The type of substituents does not exert a significant influence on the bands in this regions. In current investigation the CH stretching vibrations are experimentally found to be 2887 and 2823 cm⁻¹ in FT-IR. And theoretically observed with their PED percentages of 3103(97 %), 3088(97 %), 3086(88 %), 3074(99 %), 3066 (94 %), 3049(91 %), 3031(97 %), 3004(94 %), 2999(95 %), 2996(99 %), 2979(99 %), 2953(99 %) and 2902 cm⁻¹(99 %).

4.2.4. Carbon – Oxygen vibrations

The most important vibration of C—O stretching occurred in 1850–1550 cm⁻¹ [35]. The Title compounds were experimentally measured (FT-IR) 1734 cm⁻¹, 1621 cm⁻¹ and (FT-Raman) 1738 cm⁻¹, 1619 cm⁻¹. Theoretically anticipated in C—O stretching vibrations are 1762, 1687 and 1643 cm⁻¹, their PED contributions are 88 %, 84 % and 82 % respectively.

Fig. 2a. FT – IR spectra of 2C₂OFig. 2b. FT – Raman spectra of 2C₂O.

4.2.5. Carbon – Carbon vibrations

The spectral region spanning from 1650 to 1100 cm^{-1} is accredited to C–C vibrations in both aromatic and heteroaromatic compounds [36]. The precise positioning of the ring is contingent upon the nature of the substitution it undergoes. In present study FT-IR and FT-Raman

experimentally observed at 1542 cm^{-1} , 1294 cm^{-1} and 1541 cm^{-1} , 1294 cm^{-1} . Theoretically in 1591, 1536, 1312, 1300, 972 and 793 cm^{-1} . The percentage of PED contributions in ranges of 52 %, 51 %, 38 %, 46 %, 16 % and 60 % respectively.

Table 2

Experimental and Theoretical Vibrational Assignment of 2C2O.

Modes	Experimental Frequency (cm ⁻¹)		Theoretical Frequency (cm ⁻¹)		IR (Intensity)		Raman (Intensity)		^d PED ASSIGNMENT(%)
	FT-IR	FT-RAMAN	Unscaled	Scaled ^a	Relative	Absolute ^b	Relative	Absolute ^c	
114	3750		3753	3606	85	17	91	42	ν OH(100)
113			3684	3540	515	100	175	82	ν OH(99)
112	3240		3634	3492	34	7	64	30	ν NH(100)
111			3229	3103	1	0	105	49	ν CH(97)
110			3213	3088	22	4	72	34	ν CH(97)
109	3081		3211	3086	4	1	125	58	ν CH(88)
108			3199	3074	0	0	91	42	ν CH(99)
107			3190	3066	11	2	205	96	ν CH(94)
106			3173	3049	4	1	77	36	ν CH(91)
105	3020		3154	3031	4	1	82	38	ν CH(97)
104			3126	3004	10	2	215	100	ν CH(94)
103			3121	2999	18	3	37	17	ν CH(95)
102			3118	2996	1	0	54	25	ν CH(99)
101			3100	2979	6	1	38	18	ν CH(99)
100	2887		3073	2953	17	3	133	62	ν CH(99)
99	2823	2894	3019	2902	24	5	60	28	ν CH(99)
98	1734	1738	1834	1762	457	89	15	7	ν OC(88)
97			1756	1687	381	74	56	26	OC(88)
96	1621	1619	1710	1643	440	85	35	16	ν OC(82)
95		1582	1655	1591	202	39	154	72	ν CC(52)
94	1572		1629	1566	42	8	20	9	ν CC(55) + β CCC(14)
93	1542	1541	1598	1536	78	15	148	61	CC(51)
92			1526	1466	340	66	20	9	NC(1) + β HNC(35)
91			1517	1458	64	12	9	9	β NC(23) + β HCC(20)
90			1514	1455	3	1	13	6	ν CC(14) + β HCH(74)
89	1436	1438	1501	1442	1	0	3	2	β HCH(72)
88			1479	1421	13	3	19	9	ν CC(18) + β HCC(42)
87	1406	1409	1470	1413	3	1	8	4	β HCH(95)
86			1442	1386	34	7	14	14	ν ON(15) + β HOC(15)
85			1439	1383	18	3	10	10	β HCH(63) + τ HCCO(16)
84			1437	1381	22	4	7	8	β HCC(22) + β HCH(13) + τ HCON(20)
83	1345	1347	1382	1329	1	1	12	6	β HCC(21) + β HCO(13) + τ HCON(15)
82			1373	1320	10	6	6	3	β HCC(10) + β HCH(16) + τ HCCO(55)
81			1365	1312	19	4	91	42	ν CC(38)
80	1294	1297	1352	1300	1	4	2	2	ν CC(46)
79			1336	1284	27	5	3	1	ν CC(17) + β HOC(62)
78	1265		1318	1267	200	39	9	4	ν CC(11) + β HOC(13) + β HCC(17)
77			1301	1250	12	27	10	5	β HOC(10) + β HCC(19)
76			1288	1239	9	8	8	4	β HOC(15) + β HCC(32)
75	1225	1225	1271	1212	3	1	4	2	β HCO(36) + τ HCCC(10) + τ HCON(24)
74			1261	1212	99	19	83	39	ν CC(19) + β HOC(16)
73	1191		1230	1182	53	10	41	19	ν NC(32) + β HNC(13)
72			1223	1175	1	0	26	12	ν CC(49) + β HCC(28)
71	1158	1156	1153	1049	1	0	2	1	β HCC(72)
70			1141	1145	27	5	5	3	β HCC(10) + β HCO(19) + τ HCCC(14)
69			1190	1143	48	9	2	1	ν NC(11) + β HCC(14)
68			1181	1115	20	4	10	5	β HCC(57)
67			1161	1115	4	1	27	12	ν ON(31)
66	1096		1151	1106	141	27	1	0	ν CC(46) + β HOC(19)
65			1132	1088	2	0	2	1	τ HCCO(76)
64			1124	1080	5	1	3	1	ν NC(16) + β HCC(11)
63	1020		1080	1038	32	6	5	3	ν NC(38)
62			1076	1034	1	0	0	0	τ HCCC(82)
61			1063	1021	9	2	16	7	ν CC(30) + β HCC(25)
60	1017		1053	1012	11	2	13	6	ν CC(11) + τ HCCC(56)
59			1041	1000	9	2	24	11	τ HCCC(24) + τ HCON(10)
58			1041	1000	21	4	2	1	β HCC(11)
57			1012	972	33	6	13	6	ν CC(16)
56	954		997	958	0	0	0	0	τ HCCN(79)
55			976	938	56	11	6	3	ν OC(23) + τ HCCC(37)
54			975	937	68	13	11	5	ν OC(36) + τ HCCC(21)
53	900		942	905	4	1	2	1	ν CC(14) + τ HCCC(29) + τ HCON(15)
52	897		919	883	24	5	5	2	β CCC(27) + β CCO(10)
51			898	863	4	1	3	2	β CCC(19)
50			883	849	43	8	4	2	ν NC(11) + ν CC(14) + β CCC(10)
49			879	845	1	0	0	0	τ HCCN(73) + τ HCCC(12)
48	809		838	805	6	1	5	2	ν CC(29) + β CCC(13) + τ HCCO(38)
47			825	793	24	5	5	2	ν CC(60)
46			823	791	1	0	9	4	ν CC(48) + τ HCCO(19)
45	765		791	760	6	1	1	1	τ HCCC(13) + ω CCC(53)
44			782	752	1	0	3	2	β HCCC(79)
43	739		768	738	66	13	1	0	τ HCCN(36)

(continued on next page)

Table 2 (continued)

Modes	Experimental Frequency (cm ⁻¹)		Theoretical Frequency (cm ⁻¹)		IR (Intensity)		Raman (Intensity)		cPED ASSIGNMENT(%)
	FT-IR	FT-RAMAN	Unscaled	Scaled ^a	Relative	Absolute ^b	Relative	Absolute ^c	
42			765	735	35	7	3	1	β OCN(18)
41			757	728	9	2	1	0	τ HCCN(13) + τ CCCC(41)
40			752	723	3	1	3	1	ω ONCC 48)
39	644	668	689	662	2	0	8	4	β CNO(27) + ω CCCC(14)
38			677	650	2	0	4	2	ω OCCC(46)
37			659	634	26	5	12	6	β CCO(12)
36			652	627	96	19	1	1	τ HOCC(64)
35		597	622	598	31	6	1	0	β CCO(46)
34		578	604	581	27	5	2	1	τ HOCC(67)
33		569	588	565	20	4	2	1	β HOC(10) + β HCC(19)
32			566	544	3	1	1	1	β NCC(12) + β HOC(16)
31	560		554	532	16	3	7	3	β CCC(25)
30			528	507	13	3	1	0	β HOC 10 + τ CCCC(25)
29			493	474	15	3	1	1	τ HCCO(16) + τ HOCC(57)
28		464	477	458	20	4	1	1	τ CCCC(11)
27			455	437	5	1	11	5	β CNC(10)
26			446	429	3	1	0	0	β CON(10) + τ CC(18)
25			425	408	60	12	0	0	τ H-C(61)
24			418	402	9	2	1	0	β NCC(5) + τ HNCC(6)
23			396	381	3	1	3	1	β NCC(10) + β CCC(5)
22			383	368	7	1	0	0	β CCC(61)
21			364	350	2	0	2	1	β C=O(52)
20			321	308	6	1	0	0	β CCO(73)
19			317	304	5	1	4	2	β NCC(10)
18			285	274	4	1	1	0	β N(24)
17			281	270	6	1	1	0	β OCN(16) + β CNC(21)
16			255	245	1	0	3	1	ν CC(22) + β CCC(12)
15			230	221	3	1	1	1	β CON(11) + ω CCCC(19)
14			187	180	1	0	1	0	β CCO(27) + τ CCCC(18)
13			169	162	2	0	1	0	τ CCCC(38) + τ CNCC(13) + τ CCCC(14)
12			150	145	3	1	1	0	β CCC(15) + τ CCCO(18)
11			145	139	1	0	0	0	β NCC(11) + β CCC(14) + τ CCCO(11)
10			120	115	1	0	1	0	β CCC(16) + τ CCCO(29)
9			94	91	1	0	0	0	τ CNCC(23) + τ CCCO(27)
8			75	72	3	1	2	1	τ CCNC(63)
7			67	64	1	0	2	1	τ CCNC(40)
6			54	52	1	0	2	1	τ CCCC(12) + τ CNCC(12) + ω CCCC(18) + ω OCCN(20)
5			54	52	1	0	2	1	τ CCNC(35) + ω OCCN(19)
4			37	35	1	0	1	0	τ CCON(13) + τ CCO(54)
3			32	31	1	1	1	1	τ CCON(75)
2			23	21	2	0	1	0	τ CCON(67)
1			17	17	7	0	0	0	τ CCON(55)

^a Scaling factor: 0.961 for B3LYP/6-311+G(d,p).^b Relative IR absorption normality intensities with highest peak absorption equal to 100.^c Relative RAzMAN intensities normalized to 100.^d ν-stretching, β-Bending, τ-Torsion, ω-OCCN, plane bending.

4.2.6. Carbon – Nitrogen vibrations

The vibration of the C≡N or N=N stretching bond was determining to occur within a spectral range of 1350–1280 cm⁻¹ [37,38]. Due to the possibility of vibration mixing in this area, identifying C—N vibrations is an extremely difficult task. In title compound C—N peak observed at 1020 cm⁻¹ in experimentally and 1038 cm⁻¹ theoretically with 38 % of PED assignment.

4.3. Charge distribution analysis

MEP is a method to illustrate the 3 - dimensional charge distribution for molecules [39]. The reason for this linked to electron density [23,40]. The investigation of a multitude of biological processes and systems commonly relies on the utilization of ESP. Significant advancements have been made in various fields, including the reactive properties of nucleic acids, chemical carcinogenesis of molecule and biological recognition, as well as organic and inorganic properties of bio – molecules [41–43]. Among MEPs colors molecular structure the red represents the electron rich regions (nucleophilic attack to negative electrostatic potential) zero potential is marked as green and blue denotes electron poor constituent (The intrusion of electrophiles ESP into

positive regions). ESP escalates for the following series of Red, Orange, Yellow, Green and Blue [44]. Molecular Electrostatic Potential has been computed in the present investigation using several kinds of solvents. In every phase, oxygen atoms O2 and O4 serve as the primary sites for electrophilic attack. This is explained by the fact that they are located within the maps red areas. Conversely, the hydrogen atoms H36 and H40 exhibit noteworthy nucleophilic characteristics, thus presenting considerable nucleophilic sites as shown in Fig. 3. The compound exhibits the potential ranges of various phases $-7.192e^{-2}$ to $7.192e^{-2}$ (GAS), $-8.136e^{-2}$ to $8.136e^{-2}$ (WATER), $-8.100e^{-2}$ to $8.100e^{-2}$ (DMSO), $-8.082e^{-2}$ to $8.082e^{-2}$ (METHANOL), $-8.066e^{-2}$ to $8.066e^{-2}$ (ETHANOL) theoretically.

4.4. Frontier molecular orbital

The FMO hypothesis stands an exemplary method for effectively characterizing molecules chemical stability, which incorporates HOMO and LUMO [45]. The energy distribution and energetic behaviour of molecule and complexes can unveiled through the analysis of the HOMO – LUMO energies. This information offers important insights into the intricate workings of systems. The stability of compound is established

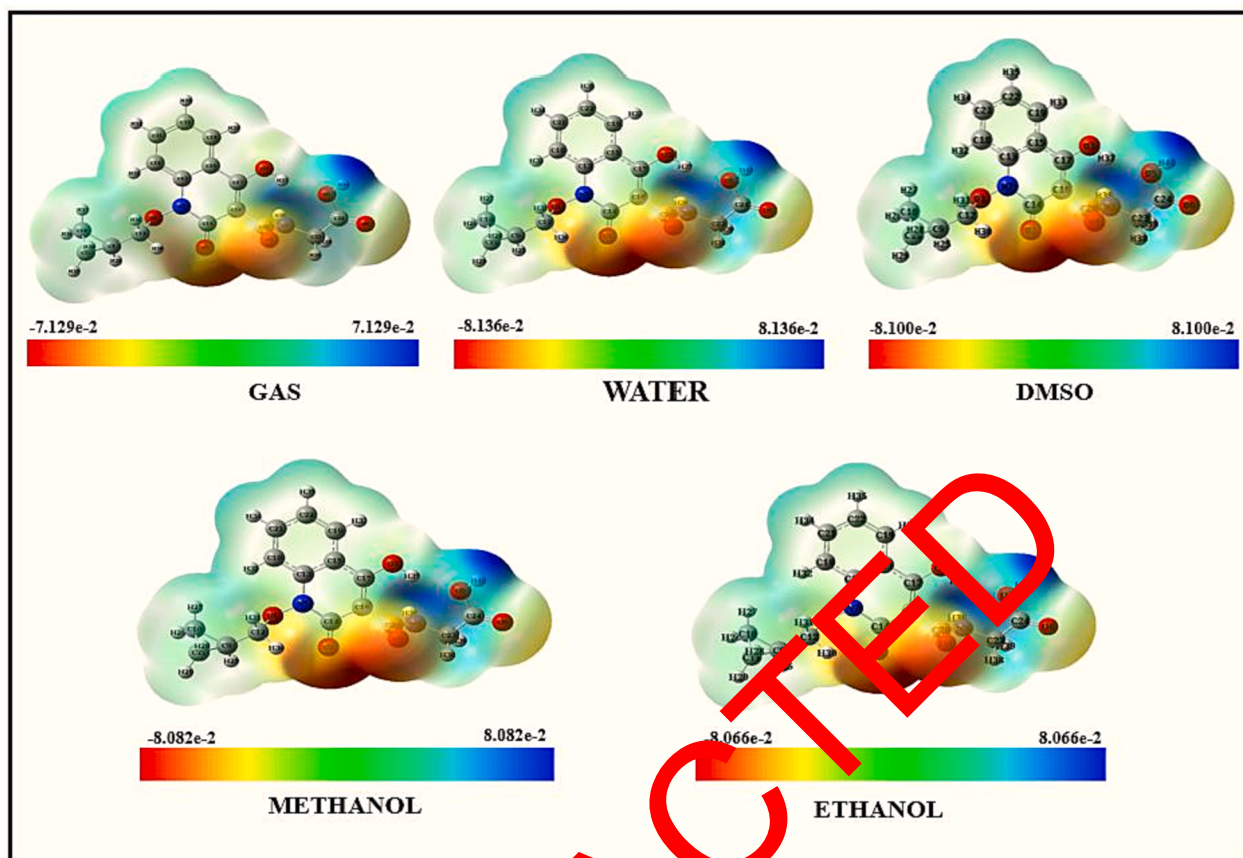


Fig. 3. Molecular Electrostatic potential for PC2O with different solvents.

by the negative magnitudes of $E_{HOMO} - E_{LUMO}$ [46,47]. Low softness or hard molecule compounds have large values of energy gap, whereas high softness or soft molecule compounds have small values of binding energy.

Hardness and molecule stability have an antagonistic relationship as shown [48] using Koopmans's theorem, the global and reactivity descriptor values are generated from the FMO energy values as shown below [49–52]. The Homo-LUMO energy diagrams are depicted in Fig. 4.

$$IP = -E_{HOMO} \quad (1)$$

$$EA = -E_{LUMO} \quad (2)$$

$$\text{Chemical Potential } (\mu) = -\frac{(IP + EA)}{2} \quad (3)$$

$$\text{Hardness } (\eta) = \frac{IP - EA}{2} \quad (4)$$

$$\text{Softness } (S) = \frac{1}{2\eta} \quad (5)$$

$$\text{Electronegativity } (\chi) = \frac{IP + EA}{2} \quad (6)$$

$$\text{Electrophilicity index } (\omega) = \frac{\mu^2}{2\eta} \quad (7)$$

The band gap values are obtained various phases like gas, water, DMSO, Methanol and Ethanol. The energy bandgap energy value of 4.5207 eV(GAS), 4.7528 eV(WATER), 4.6145 eV(DMSO), 4.6126 eV (METHANOL) and 4.6110 eV (Ethanol) are calculated. compared to other solvents aqueous(water)solution has large value of band gap

4.7528 eV. The energy values increasing order of Gas < Ethanol < Methanol < DMSO < Water. The title compound HOMO and LUMO exhibit progressively lower energy values when the solvents polarity gets stronger, this is because its possible that when Vander Waals interactions rise. Molecule stability is higher in solvents with more polarity. The ability of an element to interact with bio-molecules is indicated by molecules electrophilicity index. The greater value of electrophilicity indices for specified molecule indicated that it executes as an electrophilic agent and has a superior capacity for binding to Bio-molecules. The very minimal amount of energy needed to annihilate an atom or molecule can be identified as the Ionisation potential [53]. The change in energy that occurs when an electron is added to a neutral atom in the gas phase is referred to as electron affinity. Chemical softness and chemical potential as representative of electronegativity of complexes. Chemical hardness, electronegativity aid in predicting the formation of chemical bands as well as the chemical and physical characteristic for the compound. Global descriptors of the head compound values are listed in Table 3.

4.5. Natural bond orbital analysis

The computed bonding orbital with an enormous electron density is referred to as the natural bond orbital (NBO). NBO analysis is the promising technique use for investigating inter and intramolecular interactions [54,55]. In order to account for the interactions amongst entirely filled Lewis-type Natural bond orbital(NBOs) and partially occupied Non-Lewis NBOs, this approach utilized second-order perturbation theory to acquire energy values. This approach was employed to consider the Donor – Acceptor interactions, specifically the bond – antibond interactions [56,57]. The H-bond rationalisation is well explained by the NBO analysis. In general, it is anticipated that the

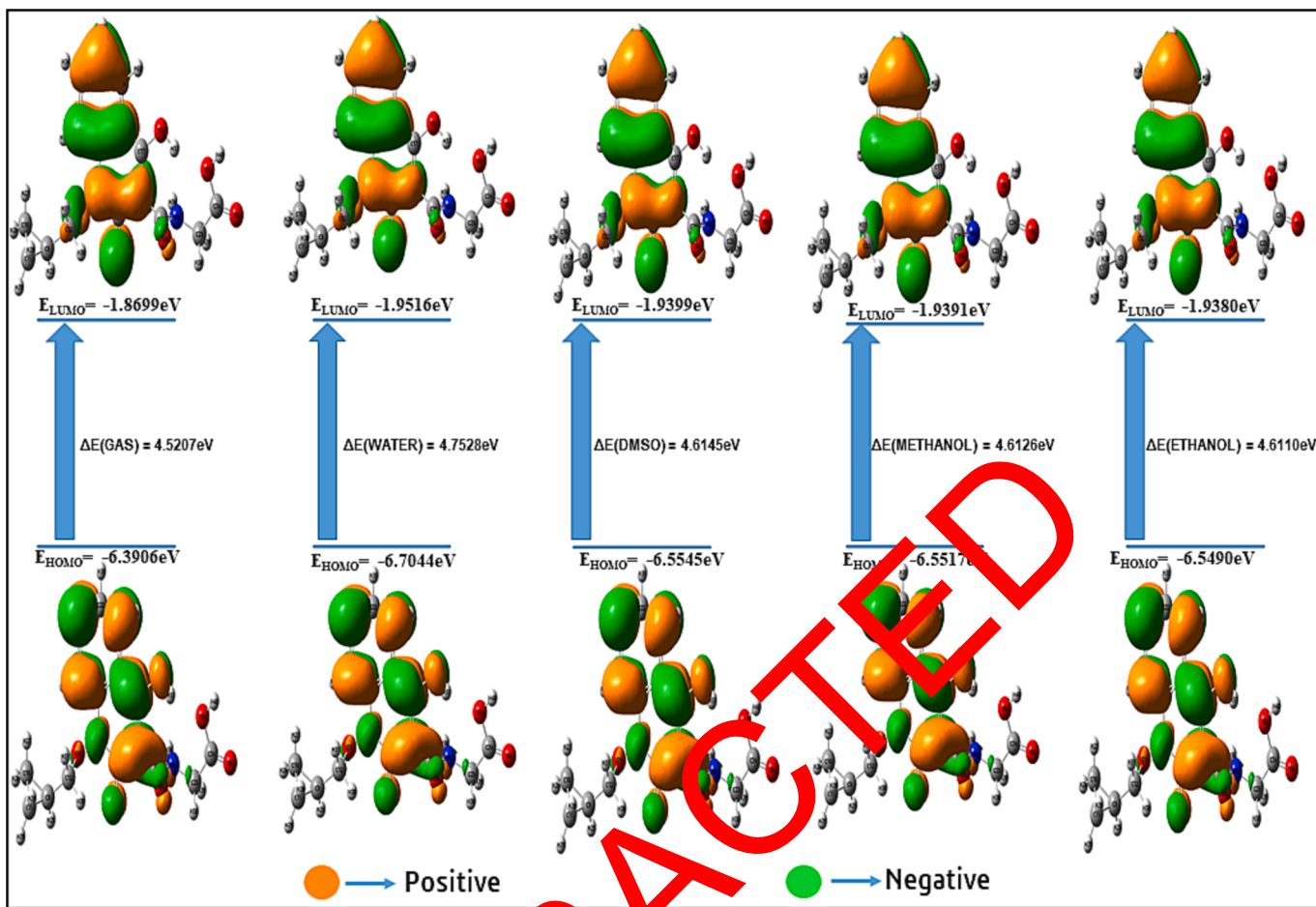


Fig. 4. HOMO-LUMO plots in different solvents of 2C2O.

Table 3
Chemical reactivity and stability description.

Parameters (eV)	GAS	WATER	DMSO	METHANOL	ACETONE	ETHANOL
HOMO	-6.3906	-6.7044	-6.5545	-6.5517	-6.5466	-6.5490
LUMO	-1.8699	-1.9516	-1.9399	-1.9391	-1.9369	-1.9380
Ionization potential	6.3906	6.7044	6.5545	6.5517	6.5466	6.5490
Electron affinity	1.8699	1.9516	1.9399	1.9391	1.9369	1.9380
Energy gap (ΔE)	4.5207	4.7528	4.6145	4.6126	4.6096	4.6110
Electronegativity (χ)	2.1303	2.3280	2.4272	2.4254	2.4217	2.4235
Chemical potential (μ)	-4.1303	-4.3280	-4.2472	-4.2454	-4.2417	-4.2435
Chemical hardness (η)	2.2604	2.3764	2.3073	2.3063	2.3048	2.3055
Chemical softness (S)	0.2212	0.2104	0.2167	0.2168	0.2169	0.2169
Electrophilicity index (ω)	3.7735	3.9412	3.9091	3.9074	3.9032	3.9053

contact between proton acceptor and proton donor considered as the conjugative charge transfer that allows hydrogen bonds to form. The H...Y bonds (X-H...Y) ability to elongate and contact depends heavily on the quantity of charge transfer [58–61]. The stabilisation Energy $E^{(2)}$ accompanying through delocalisation from donor (i) to acceptor(j) is evaluated as follows,

$$E^{(2)} = \Delta E_{ij} = q_i \frac{F(i,j)^2}{\varepsilon_i - \varepsilon_j} \quad (8)$$

Where q_i represents occupancy of donor orbital. $\varepsilon_{i,j}$ are the diagonal component and Off-diagonal fock matrix component denoted as $F(i, j)$. The intensity of connection amongst electron donor and an acceptor, inclination for the electron donor to donate electrons to acceptor of electron, range of conjugation for entire system increase with increasing of $E^{(2)}$. In Table 4, the results of perturbation energies of significant

Donor – Acceptor interactions are shown. The head compounds interactions between $\sigma(O6-C24)$ and antibond $\pi^*(C21-C22)$ have the strongest stabilisation energy(E^2) value of 598.8 kcal/mol. The other important interactions of $\sigma(N28-C20)$ to $\pi^*(C21-C22)$ and $\sigma(O5-H40)$ to $\sigma^*(C23-C24)$ and $\pi^*(C13-C18)$ to $\pi^*(C15-C19)$ are giving the strong stabilisation energy values of 544.14, 245.51 and 203.65 kcal/mol respectively. The lone pair interaction between LP (1) O5 to $\sigma^*(C23-C24)$ gives the $E^{(2)}$ value of 154.91 kcal/mol. The donor $\pi^*(C16-C17)$ to acceptor $\pi^*(O2-C14)$ occur the stabilisation energy of 132.65 kcal/mol.

4.6. Mulliken atomic charges

Molecular systems require an understanding of the Mulliken atomic charge distribution for performing quantum chemistry. Net atomic

Table 4

Second – order perturbation Fock-matrix energy calculation of 2C2O.

Donor NBO(i)	Type	ED/e	Acceptor NBO(j)	Type	ED/e	^a E ⁽²⁾ kcal/mol a.u.	^b F(j)-E(i) a.u.	^c F(i,j) a.u.
O6—C24	σ	1.99665	C21—C22	π*	0.3764	598.8	0.31	0.425
N8—C20	σ	1.98971	C21—C22	π*	0.3764	544.14	0.02	0.111
O5—H40	σ	1.98721	C23—C24	σ*	0.0755	245.51	2.88	0.763
C13—C18	π*	0.41046	C15—C19	π*	0.4256	203.65	0.02	0.082
O5	LP(1)	1.9715	C23—C24	σ*	0.0755	154.91	2.83	0.598
C16—C17	π*	0.28321	O2—C14	π*	0.363	132.65	0.02	0.076
O5—C24	σ	1.99604	C23—H38	σ*	0.0148	131.08	3.15	0.575
O5—H40	σ	1.98721	C23—H38	σ*	0.0148	104.7	2.93	0.495
C16—C17	π*	0.28321	C15—C19	π*	0.4256	103.62	0.02	0.07
O5—H40	σ	1.98721	C23—H39	σ*	0.01	100.15	2.7	0.464
O5—C24	σ	1.99604	C23—C24	σ*	0.0755	86.53	3.1	0.471
O5—C24	σ	1.99604	C23—H39	σ*	0.01	82.85	2.92	0.439
O3—C17	σ	1.99245	C21—C22	π*	0.3764	54.75	0.13	0.083
O5	LP(1)	1.9715	C23—H39	σ*	0.01	53.85	2.65	0.339
O5—H40	σ	1.98721	C21—H34	σ*	0.0131	53.42	0.99	0.205
O5—C24	σ	1.99604	C21—H34	σ*	0.0131	51.74	1.21	0.223
N7	LP(1)	1.63133	O2—C14	π*	0.363	48.37	0.3	0.108
O5	LP(1)	1.9715	C21—H34	σ*	0.0131	45.50	0.94	0.186
N8	LP(1)	1.71645	O4—C20	π*	0.2447	44.21	0.33	0.11
O5	LP(2)	1.83685	O6—C24	π*	0.1931	41.85	0.35	0.109
N7	LP(1)	1.63133	C13—C18	π*	0.4105	41.48	0.29	0.098
O3	LP(2)	1.8448	C16—C17	π*	0.2832	39.78	0.34	0.105
O6—C24	σ	1.99665	C21—H34	σ*	0.0131	36.29	1.39	0.201
O5—C24	σ	1.99604	C14—C16	σ*	0.0602	35.35	1.29	0.194
O5	LP(1)	1.9715	C23—H38	σ*	0.0131	35.00	2.88	0.285
C21—C22	π*	0.37644	C21—H34	σ*	0.0131	34.62	1.08	0.391
O6	LP(2)	1.83513	O5—C24	σ*	0.1039	34.56	0.6	0.13
C23—C24	σ	1.97847	C21—H34	σ*	0.0131	33.4	0.99	0.163
O5—H40	σ	1.98721	C14—C16	σ*	0.0602	33.39	1.07	0.171
C21—C22	π*	0.37644	C23—C24	σ*	0.0755	31.28	2.97	0.573
O2	LP(2)	1.85457	N7—C14	σ*	0.104	29.79	0.63	0.124
O5—H40	σ	1.98721	C16—C20	σ*	0.0602	29.12	1.02	0.156
O5—C24	σ	1.99604	C16—C20	σ*	0.066	29.1	1.24	0.172
O5—C24	σ	1.99604	C11—H28	σ*	0.012	27.32	1.3	0.169
O4—C20	σ	1.99291	C21—C22	π*	0.3764	26.76	0.21	0.074
O5	LP(1)	1.9715	C14—C16	σ*	0.0602	26.73	1.03	0.149
O4	LP(2)	1.85311	C16—C20	σ*	0.066	26.01	0.55	0.109
O4	LP(2)	1.85311	N8—C20	π*	0.0829	25.73	0.7	0.122
C21—C22	π	1.61753	C14—C19	π*	0.4256	25.01	0.27	0.075
O5	LP(1)	1.9715	C16—C20	σ*	0.066	24.64	0.97	0.139
C15—C19	π	1.62386	C13—C18	π*	0.4105	24.52	0.26	0.072
C15—C19	π	1.62386	C16—C17	π*	0.2832	24.12	0.26	0.072
C16—C17	π	1.79734	C9—C14	π*	0.363	23.68	0.3	0.079
O2	LP(2)	1.85457	C14—C16	σ*	0.0602	23.68	0.59	0.108
C21—C22	π*	0.37644	C14—C16	σ*	0.0602	23.09	1.17	0.314
O6—C24	σ	1.99665	C14—C16	σ*	0.0602	22.68	1.48	0.166
C21—C22	π*	0.37644	C16—C20	σ*	0.066	22.66	1.11	0.301
O5—H40	σ	1.98721	C11—H28	σ*	0.012	22.19	1.08	0.139
C21—C22	π	1.61753	C13—C18	π*	0.4105	19.99	0.26	0.064
C23—C24	σ	1.97847	C14—C16	σ*	0.0602	19.97	1.08	0.132
O6—C24	σ	1.97847	C16—C20	σ*	0.066	19.49	1.42	0.151
C23—C24	σ	1.97847	C16—C20	σ*	0.066	18.27	1.02	0.123
C21—C22	π*	0.37644	C23—H38	σ*	0.0148	17.5	3.02	0.464
C13—C18	π	1.6031	C15—C19	π*	0.4256	17.3	0.28	0.063
O6	LP(1)	1.9789	C21—H34	σ*	0.0131	16.57	0.99	0.114
C21—C22	π*	0.37644	C23—H39	σ*	0.01	14.66	2.79	0.411
O5	LP(1)	1.9715	C11—H28	σ*	0.012	14.17	1.04	0.109
O5	LP(2)	1.83685	C23—H39	σ*	0.01	13.38	2.35	0.165
O6—C24	σ	1.99665	C11—H28	σ*	0.012	13.35	1.49	0.126

^a E⁽²⁾ Energy of Hyper-conjugative interaction.^b Energy difference between I and J NBO orbitals.^c F(i,j) Fock matrix element between I and J NBO orbitals.

population of molecule can be reckoned by the Mulliken charges [62]. The natural charge distribution within molecular systems is intricately linked to properties such as polarizability, electronic structure, and dipole moment, and a wide range of other characteristics. Fig. 5 shows Graphical representation of the atom numbers and calculated atomic charges. The current study molecule maximum positive value exhibits the C16 atom of the value of 0.831. Meanwhile, C19 atom exhibits maximum negative charges. The title compounds hydrogen atoms are all

in positive charge. Maximum positive value hydrogen atom is H37 for the value of 0.456 likely it is connected with the electronegative O3 atom.

4.7. Local reactivity descriptor

Electronegativity(χ), Softness(S) and hardness(η) stands global characteristic of molecular reactivity system. The Fukui and Local



Fig. 5. Graphic representation of Mulliken atomic charges.

softness, which is commonly employed parameter characterizing reactivity, is contemplated to be the rate of change of electron density with regards variations in electron count, while keeping the positions of nuclei constant [63–65]. The chemical reactivity and selectivity [66] of a compound may be predicted using Fukui function, which indexes reveal a molecules tendency to acquire or loss electrons. With this understanding, it becomes feasible to ascertain whether an atom within a molecule is more prone to being attacked by a nucleophile or electrophile. A molecule accepts an electron, the fukui function is (f_r^+) known as nucleophilic attack index. The Fukui function(f_r^-) is used which is known for electrophilic attack. The formulas listed below can be utilized for calculating FUKUI functions.

$$\text{Nucleophile } f^+(r) = q_{r(N+1)} - q_{r(N)} \quad (9)$$

$$\text{Electrophile } f^-(r) = q_{r(N)} - q_{r(N-1)} \quad (10)$$

$$\text{Radical } f(0) = \frac{q_{r(N+1)} - q_{r(N-1)}}{2} \quad (11)$$

(N) is neutral, (N – 1) is cationic chemical type, $q_r \rightarrow r^{\text{th}}$ atomic site atom charge, (N + 1) is anionic. [0, +, –] indicating radial, nucleophilic, electrophilic attack respectively. Dual descriptor is the combination for fukui functions [67] $f^+(r)$ and (f_r^-) are

$$\Delta f(r) = f^+(r) - f^-(r) \quad (12)$$

The site nucleophilic if $\Delta f(r)$ is greater than zero and electrophilic if $\Delta f(r)$ less than zero. The reactive site nature may be identified using the dual descriptor in this manner. Table 5 exposition atom H40 has a

greater dual descriptor negative value –0.290 displays they are high electrophile. Hence, sequence of electrophile exposure as H40 > C20 > C17 > H39 > C21 > C19 > H38 > C13 > C12 > H33 > C9 > C24 > H32 > H36 > H34 > H30. The atom C23 is highly dual descriptor positive value 0.291 exhibits more nucleophile attack, while, C23 > O2 > C22 > H37 > C15 > N7 > O1 > C14 > H31 > C18 > O4 > O5 > H35 > C16 > H27 > C11 > H28 > H26 > H29 > O3 > C10 > O6 > N8 > H25 are grouped according to decreasing order of nucleophilic attack. These findings demonstrate the reactive characteristics for title compound 2C2O.

4.8. UV-Vis spectrum analysis

Application of the technique of UV-Vis spectroscopy, the static and dynamic characteristics as well as the electronic transitions of the title chemical are investigated. The theoretical spectra of the head compound utilizing the Gas phase and various phases of solvents including Methanol, Water, DMSO, and Ethanol are obtained the Time-Dependent – DFT technique and Integral Equation Formalism PCM (IEFPCM) method [68]. The theoretical UV-Vis spectra as shown in Fig. 6 in accordance with the largest band gap, the valance electrons closely encircle the nucleus [69]. Table 6 originated with the information concerning wavelength, bandgap, Energy, oscillator strength, symmetry and contribution. The title compound exhibits a gas phase electronic absorption peak at 262.2 nm, corresponding to a maximum peak value. The band gap of this compound is measured at 4.61 eV, and its energy is determined to be 37145.86 cm⁻¹. Notably, the electronic absorption from the FMO of this compound is significantly assisted, accounting for

Table 5

Local softness and Dual descriptor for title compound 2C2O.

Atoms	Mulliken atomic charges			Fukui functions			Δf_r	local softness		
	0, 1 (N)	N + 1 (-1, 2)	N-1 (1,2)	f_r^+	f_r^-	f_r^0		$sr + f_r^+$	$sr \cdot f_r^-$	$sr \cdot f_r^0$
O1	0.378608	0.450191	0.34933	0.072	0.029	0.050	0.042	0.016	0.006	0.011
O2	-0.248605	-0.073055	-0.324105	0.176	0.076	0.126	0.100	0.038	0.016	0.027
O3	-0.307699	-0.269112	-0.341469	0.039	0.034	0.036	0.005	0.008	0.007	0.008
O4	-0.218043	-0.171011	-0.247225	0.047	0.029	0.038	0.018	0.010	0.006	0.008
O5	-0.289739	-0.297929	-0.266424	-0.008	-0.023	-0.016	0.015	-0.002	-0.005	-0.003
O6	-0.250069	-0.216127	-0.280544	0.034	0.030	0.032	0.003	0.007	0.007	0.007
N7	-0.340972	-0.298521	-0.338247	0.042	-0.003	0.020	0.045	0.009	-0.001	0.004
N8	-0.131536	-0.119496	-0.141205	0.012	0.010	0.011	0.002	0.003	0.002	0.002
C9	0.30471	0.29693	0.303161	-0.008	0.002	-0.003	-0.009	-0.002	0.000	-0.001
C10	-0.349697	-0.333664	-0.361143	0.016	0.011	0.014	0.005	0.003	0.002	0.003
C11	-0.364962	-0.359298	-0.364418	0.006	-0.001	0.003	0.006	0.001	0.000	0.001
C12	-0.663726	-0.738924	-0.607519	-0.075	-0.056	-0.066	-0.019	-0.016	-0.012	-0.014
C13	-0.371419	-0.397736	-0.384446	-0.026	0.013	-0.007	-0.039	-0.006	0.003	-0.001
C14	0.193555	0.210224	0.209636	0.017	-0.016	0.000	0.033	0.004	-0.004	0.000
C15	1.061488	1.102477	1.093821	0.041	-0.032	0.004	0.073	0.009	-0.007	0.001
C16	0.565466	0.583593	0.561211	0.018	0.004	0.011	0.014	0.004	0.001	0.002
C17	0.469959	0.519917	0.344114	0.050	0.126	0.088	-0.038	0.011	0.027	0.019
C18	-0.609857	-0.583874	-0.617589	0.026	0.008	0.017	0.118	0.006	0.002	0.004
C19	-0.86416	-0.870995	-0.914061	-0.007	0.050	0.022	-0.065	-0.001	0.011	0.005
C20	-0.476626	-0.440119	-0.613639	0.037	0.137	0.087	-0.101	0.008	0.030	0.019
C21	-0.300717	-0.273821	-0.390203	0.027	0.089	0.058	-0.063	0.006	0.020	0.013
C22	-0.58055	-0.513448	-0.566101	0.067	-0.014	0.021	0.082	0.015	-0.003	0.006
C23	-0.28322	-0.291821	-0.055258	-0.009	-0.228	-0.118	0.219	-0.002	-0.050	-0.026
C24	0.146189	0.142236	0.143148	-0.004	0.003	0.000	-0.001	-0.001	0.001	0.000
H25	0.241139	0.257005	0.226551	0.016	0.015	0.015	0.001	0.003	0.003	0.003
H26	0.151407	0.18038	0.128512	0.029	0.023	0.026	0.006	0.006	0.005	0.006
H27	0.126839	0.125018	0.136374	-0.002	-0.010	-0.001	0.008	0.000	-0.002	-0.001
H28	0.13621	0.151596	0.126914	0.015	0.009	0.012	0.006	0.003	0.002	0.003
H29	0.159815	0.189955	0.135269	0.030	0.025	0.027	0.006	0.007	0.005	0.006
H30	0.207685	0.215296	0.198826	0.008	0.009	0.008	-0.001	0.002	0.002	0.002
H31	0.151923	0.184377	0.138413	0.032	0.014	0.023	0.019	0.007	0.003	0.005
H32	0.180966	0.227887	0.127223	0.047	0.014	0.050	-0.007	0.010	0.012	0.011
H33	0.170566	0.21986	0.10239	0.001	0.068	0.059	-0.019	0.011	0.015	0.013
H34	0.181235	0.241271	0.119892	0.061	0.061	0.061	-0.001	0.013	0.013	0.013
H35	0.164996	0.234004	0.110573	0.069	0.054	0.062	0.015	0.015	0.012	0.013
H36	0.317207	0.325189	0.303615	0.008	0.014	0.011	-0.006	0.002	0.003	0.002
H37	0.541287	0.543641	0.615619	-0.002	-0.074	-0.036	0.077	0.001	-0.016	-0.008
H38	0.264043	0.273619	0.20461	-0.010	0.059	0.035	-0.050	0.002	0.013	0.008
H39	0.205904	0.2284	0.12398	0.022	0.097	0.060	-0.074	0.005	0.021	0.013
H40	0.330366	0.345887	0.25005	0.016	0.305	0.160	-0.290	0.003	0.067	0.035

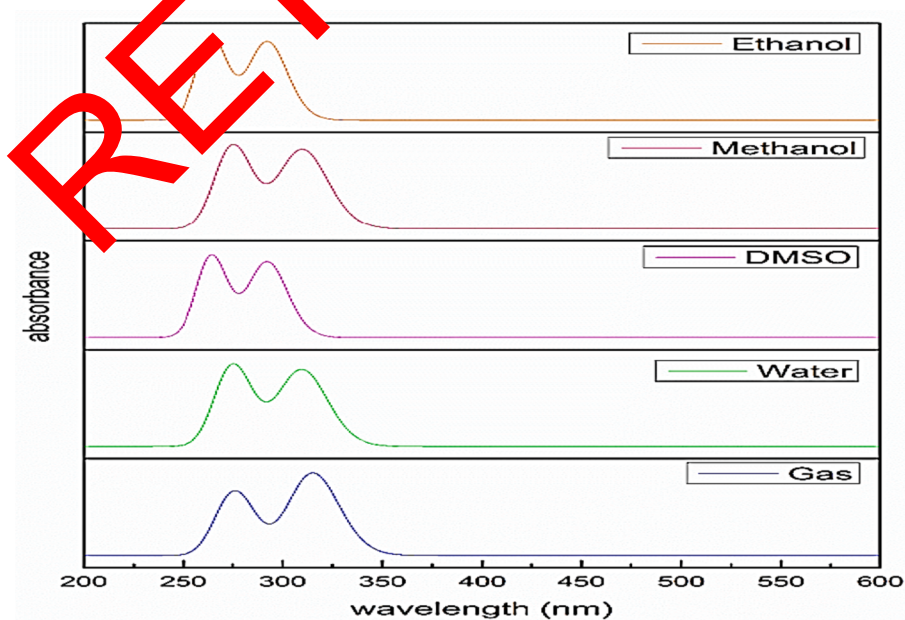


Fig. 6. Ultra Violet – Vis spectra of 2C2O with different solvents. (For interpretation of the references to color in this figure legend, the reader is referred to the web version of this article.)

Table 6

Computed electronic states of 2C2O with time-dependent-DFT method.

Solvents	Wavelength (nm)	Band Gap ΔE (eV)	Energy (cm ⁻¹)	Oscillator strength (f)	Symmetry	Major Contribution
GAS	314.920	3.94	31754.048	0.1034	Singlet-A	HOMO \rightarrow LUMO (93 %)
	276.639	4.48	36148.156	0.0731	Singlet-A	H-2 \rightarrow LUMO (13 %), H-1 \rightarrow LUMO (70 %), HOMO \rightarrow L + 2 (12 %)
	269.209	4.61	37145.864	0.0107	Singlet-A	H-2 \rightarrow LUMO (81 %)
WATER	309.504	4.01	32309.764	0.1268	Singlet-A	HOMO \rightarrow LUMO (94 %)
	274.946	4.51	36370.765	0.1357	Singlet-A	H-1 \rightarrow LUMO (83 %), HOMO \rightarrow L + 1 (14 %)
	252.601	4.91	39588.111	0.0005	Singlet-A	H-3 \rightarrow LUMO (45 %), H-2 \rightarrow LUMO (44 %)
DMSO	309.968	4	32261.371	0.1332	Singlet-A	HOMO \rightarrow LUMO (94 %)
	275.245	4.51	36331.244	0.1451	Singlet-A	H-1 \rightarrow LUMO (84 %), HOMO \rightarrow L + 1 (13 %)
	252.905	4.9	39540.524	0.0006	Singlet-A	H-3 \rightarrow LUMO (43 %), H-2 \rightarrow LUMO (46 %)
METHANOL	309.728	4	32286.374	0.1268	Singlet-A	HOMO \rightarrow LUMO (94 %)
	274.977	4.51	36366.733	0.1346	Singlet-A	H-1 \rightarrow LUMO (83 %), HOMO \rightarrow L + 1 (14 %)
	253.205	4.9	39493.744	0.0006	Singlet-A	H-3 \rightarrow LUMO (41 %), H-2 \rightarrow LUMO (48 %)
ETHANOL	309.991	4	32258.951	0.1294	Singlet-A	HOMO \rightarrow LUMO (94 %)
	275.117	4.51	36348.182	0.1381	Singlet-A	H-1 \rightarrow LUMO (83 %), HOMO \rightarrow L + 1 (13 %)
	253.520	4.89	39444.544	0.0006	Singlet-A	H-3 \rightarrow LUMO (39 %), H-2 \rightarrow LUMO (50 %)

81 % of the observed absorption [70]. The others like aqueous, Dimethyl Sulfoxide, Methanol and Ethanol possessing the greatest wavelength of 252.6, 252.9, 253.2 and 253.5 nm respectively.

4.9. ELF and LOL

In order to understand electron localization, ELF is an authentic concept [40]. Considering kinetic energy density as its foundation, binding description is the localized orbital location. ELF and LOL are related to each other molecularly [71]. Electron localization may be determined using Pauli repulsion on two electrons with similar spins. Superior and underneath limits of ELF are one and zero. Red denoting highest levels and blue denoting lower values [72]. In title compound the hydrogen atoms (H35, H33, H37 and H27) shows in red exhibits the largest Pauli repulsion, whereas the weakest was discovered close to carbon and oxygen atoms (C22, C19, C15, C17, C20, C12, O3, O5 and O6) show in blue region. Covalent regions are reflected by highest LOL

value which shown in Red -ve regions connecting the valence and the inner shells, which experience a lack of electrons, are linked by low LOL values. These low LOL values are depicted in blue [73]. The 2D ELF and LOL portrayal are depicted in Fig. 7.

4.10. Reduced density gradient analysis

NCI performs a significant portion in the study for chemical and organic systems. The NCI offers an extensive analysis regarding attractive (bonding) and repulsive (non – bonding) interactions within a research molecule, presenting comprehensive details on these aspects [74]. Non-covalent interactions between intra and intermolecular components are investigated in this approach in accordance with density of electrons and their derivatives. RDG analysis only displays the location of these interactions and the depictions of them in graphics. It may be quite helpful for understanding the impact and type of interactions. Sign (λ .2) $\rho \approx 0$, Sign (λ .2) $\rho > 0$, and Sign (λ .2) $\rho < 0$ accordingly are used

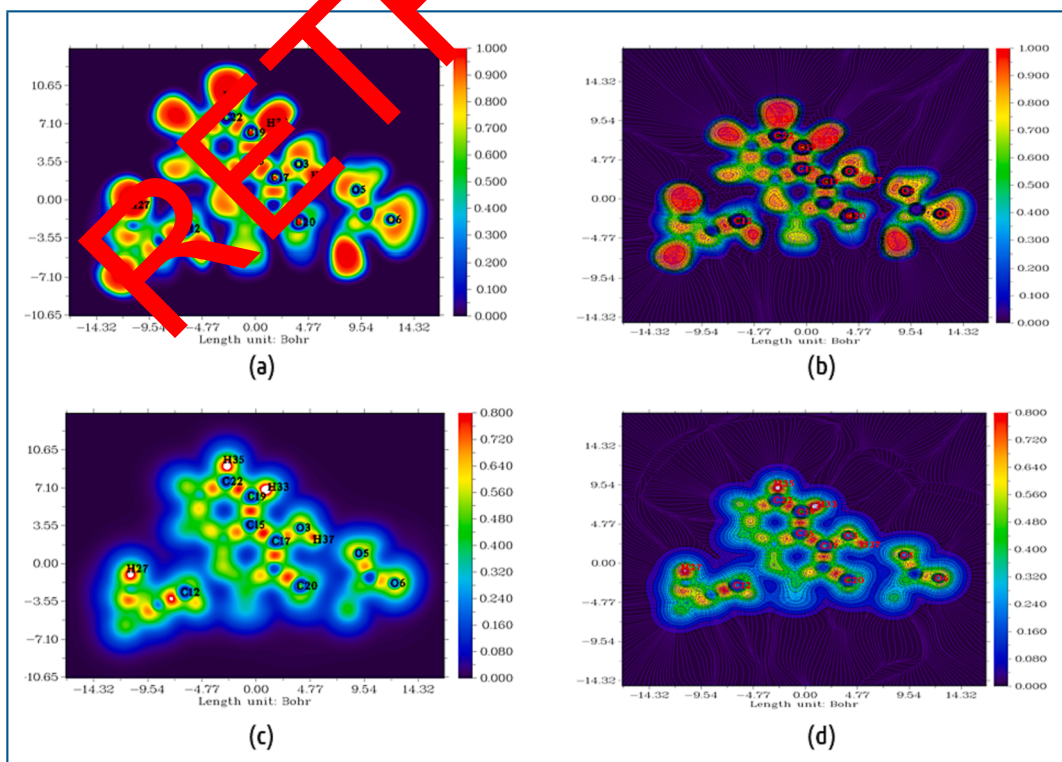


Fig. 7. (a) and (b) ELF map and colour filled map with gradient lines; (c) & (d) LOL map and colour filled map with gradient lines of 2C2O in the GAS phase.

to denote Vander Waals, repulsive and attractive interactions [75,76]. Fig. 8 depicts the three-dimensional RDG iso-surface densities and the 2D scatter plot of the title compound. Strong hydrogen bonds are responsible for the more advantageous interaction portrayed in the blue highlighted region of the RDG scatter figure between -0.05 to -0.023au . The steric effect is highlighted shiny colour of red at the core of ring of aromatics, these the beneficial zones of the scatter plot make quite evident from 0.013 to 0.05au . Vander Waals interactions are visible in the RDG plot betwixt ranges from -0.01 to -0.018a.u. and may also be detected in areas with a green color.

4.11. Bioactivity score prediction

The advantageous effects of medications on living things are referred to as pharmacological activity. A drug is something that binds to some biological substances. Receptors, Proteins, Enzymes and ion – channels are frequently used as bio – targets. The term target of drug can also apply to the biological target. The bio activity score of the complexes was determined by taking into account a number of factors including G – protein coupled receptors, Kinase and Protease inhibition and Enzyme inhibition, nuclear receptors ligand, ion-channel modulation. Through the use of online, all variables were determined. For title compound the biological activity was estimated using (<https://www.molinspiration.com>).

An organic compounds bio – activity score is classified as active if it is larger than zero, moderately active if it is between (-5 and 0) and ineffective if it is less (-5). GPCR ligand activity is $0.04 > 0$, the compound 2C2O is extremely active. Ion channel modulator value of the title compound is $0.14 > 0$ is active. Kinase inhibitor value of the compound is $0.07 > 0$ says the compound is active. Nuclear receptor ligand value $-0.23 > 0$ shows is moderately active. Protease inhibitor and enzyme inhibitor values of $0.03 > 0$ and $0.23 > 0$ that indicates the compound is active [77]. Table 7 summarises the title compounds probable bio activity score. It is evident from this that the compound possesses the qualities necessary for it to function as a medication.

4.12. Drug likeness

Drug likeness is a qualitative concept employed in the creation of pharmaceuticals [78]. It is defined as reflecting the equilibrium of a compounds molecular characteristics, which impact its pharmacodynamics, pharmaco-kinetics, and ADME in the human body [79]. For evaluating drug-likeness, several rules have been proposed. Veber rules [80], Lipinski's rule of five [81] and lipophilicity indices [82,83] are the most often employed and proven to be extremely effective and

Table 7

Title compound 2C2O prediction score of bio – activity.

GPCR ligand	Ion channel modulator	Kinase inhibitor	Nuclear receptor ligand	Protease inhibitor	Enzyme inhibitor
0.04	0.14	0.07	-0.23	0.03	0.23

>0 = active, (-5 to 0) = moderately active, <-5 = inactive.

efficient. These serve as general recommendations rather than definitive standards to determine if a molecule is drug – like or not. Table 8 provides a summary of the derived specifications and a comparison to Lipinskis results. Swiss ADME web tool is used to evaluate the results [84]. According to the rule, the majority of complexes log p values of five or less, ten or fewer Hydrogen bond acceptor, maximum of five donors of Hydrogen bonds, a molecular mass no >500 Daltons and fewer than ten rotatable bonds. A medication that is active when taken orally often violates the requirements just once. These studies findings indicate that the title compounds(ligand) oral availability is good and that is meets the specified requirements.

4.13. Molecular docking analysis

Molecular docking has emerged as a highly favoured technique in the realm of researching the correlation between structure – activity relationships and development of drugs. This approach is renowned for its ability to generate exceptionally accurate outcomes. It is possible to get the ligand and macromolecules binding energy and location, and the ligands force with the complex target molecular (receptors) [85,86]. The study key molecular processes, including ligand binding techniques, the stabilization of ligand – receptor complexes through interactions between molecules and predictions of ligand – receptor complex binding affinities are all covered by molecular docking. Because of this, molecular docking is extremely important for the creation of pharmaceuticals [87,88]. The target proteins for anemia in chronic renal illness (7KPI, 5MWP, 4NJ8, 6RTX) these were obtained through the RCSBs protein

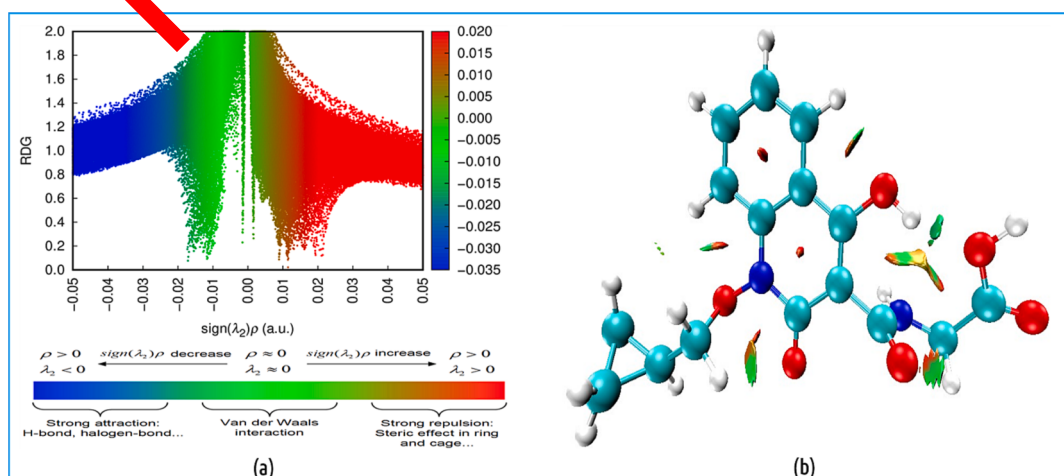


Fig. 8. (a) Plots of the RDG multiplied by $\text{sign}(\lambda_2)\rho$; (b) RDG with NCI interactions on the 2C2O Molecular surface.

data bank. Research molecules (ligand) structure has been optimised with the aid of DFT technology and the ligands PDB format was generated.

The Auto Dock applications, which may discover the best binding position for interactions between proteins and ligands, was used to carry out this docking investigation. Tables 9 and 10 and Figs. 9a and 9b list and display several binding properties, including Binding energy, reference RMSD rate, Electrostatic energy, Intermolecular energy, inhibition activity etc. Hydrophobic and hydrogen bonds interactions (C – H and conventional hydrogen bonds) were measured by utilizing the binding residues, and the measured distances are presented in 2D image and summarised in table.

As a consequence of docking, proteins 7KPI, 5MWP, 4NJ8, and 6RTX reacted well with the title chemical, with good binding energies of (-7.08 , -6.39 , -5.52 , and -5.26 kcal/mol). The complex of SP0P MATH domain (PDB-7KPI) which contains the title compound has the maximum binding value (-7.08 kcal/mol) and several interactions. For this compound three conventional hydrogen bond discovered between the residues of the protein at ALA61 and LYS64 and the functional group of CO. four alkyl (LEU65, VAL30, VAL163, LYS28) interactions has been identified with the distance of 5.15 , 4.09 , 3.76 and 4.32 Å respectively. Moreover, π -alkyl (LEU65, PRO94 and VAL98) interactions was detected with the distance of 4.29 , 5.26 , 4.85 and 4.77 Å. and also the other protein complexes are good binding properties such more conventional hydrogen bond, carbon-hydrogen bonds and weak interactions. These results shows that the title molecule (ligand) was good activity against the anemia of chronic kidney disease.

4.14. Molecular dynamics simulations

The MD modelling technique was employed to scrutinize the structural coherence of the docked compounds. Modelling protein–ligand complex with in simulated physiological conditions insilico enables the anticipation of both the varied interactions and the stericalness of protein connections. The GROMACS 5.1 [89] program collaborate to carry out the task MD simulator, and details regarding the attributes and parameters of the ligand were acquired from the Swiss Protein database. [90] illustrating the solvation of protein – ligand complexes, a new box of dimensions 1.0 nm is sketched to represent the distance involved. Additionally, the stability and dependability of a composite produced under circumstances of constant pressure, temperature, and particle count were evaluated by exploiting Molecular Dynamics (MD) at a 1 ns timeframe.

The RMSD pathway quantifies the root mean square variation of the complex [91] encompassing both protein and ligand components. The structural stability of the macro-molecular system is conferred by the ligands attachment to the active region of the receptor. Fig. 10(a) exhibits the RMSD data pertaining to the ligand compounded 7KPI, 5MWP, 4NJ8, and 6RTX. Among the proteins analysed, 7KPI, 5MWP, and 4NJ8 exhibit variations within the range of 0.03 nm, whereas protein 6RTX demonstrates a variation of 0.22 nm. Owing to the distinct range of variability evident in protein–ligand complexes, the protein reveals heightened stability. A compelling evidence of stability of molecular

system is provided by the estimated RMSD values for each protein–ligand complexes, which are closely in conformity with the original value.

RMSF is used to analyse the conformational variations of the protease at the different temperature as well as the atomic position fluctuations in the presence of ligands of amino acid ions. [92] A large RMSF value suggests that the protein – ligand complex is more flexible, even while a low RMSF value indicates restricted mobility. Fig. 10(b) illustrates that proteins display the highest fluctuations, reaching approximately 0.21 nm, whereas the fluctuations in 4NJ8 protein are comparatively minimal. This indicates a reduction in the protein stability as a result of ligand binding. Consequently, all proteins demonstrate heightened fluctuations affirming their stability.

R_g is a representation of the distance within the protease-ligand complex between the centre of mass and the rotating axis. Lower R_g value indicates increases stability and large denotes increases mobility. [93] Each complex displayed a consistent R_g profile, and calculated complexes exhibited reduced loss of disparity as illustrated in Fig. 10 (c). The protein–ligand complexes compactness is emphasized by the remarkable consistency of 4NJ8 when compared to the other proteins.

5. Conclusion

The optimized molecular characteristics, bond length and bond angle has been determined utilizing high level basis set. Experimental and theoretical FT-IR and FT-Raman spectra in great detail and Potential Energy Distribution results were utilized to designate various vibrational modes. The molecules chemical reactivity and biological activity have been shown by the investigation of HOMO – LUMO evaluation in the solvents aqueous, Dimethyl sulfoxide, methyl alcohol, ethanol additionally the gas, among the aforesaid, the solvent water has the largest bandgap energy value. The stabilisation energy via NBO technique has been used to explain the intra and intermolecular processes. The compounds chemical stability has been assessed by analysing the energy gap through UV analysis and MEP studies in both solvated and gas phases. The reactive regions of the molecule were examined separately, with the maximal peak achieved during the gaseous phase of the UV study. Using fukui functions the locations of electrophilic and nucleophilic has been identified. ELF and LOL diagrams, using Multi-wave function, were used to clarify the peculiarities of surface predictions dependent on covalent bonds. Furthermore, the scatter graph of the RDG analysis was used to identify the strong bonds of hydrogen as well as weak and steric repulsive regions. Lipinskis criterion is supported by the criteria discovered in drug similarity, demonstrates title molecule regarded as a drug. Additionally, bioactive score prediction was investigated. The pharmacological characteristics of the compound have been further confirmed. Computational investigation, such as molecular docking with potential receptors, can be used to estimate the complete action range for physiologically lively compound. This study conclusively shows how an inhibitor effects a target molecule considering its binding energy and interactions with the selected proteins. The exploration of RMSD, Radius of gyration, and RMSF in the MD simulation research supports the premise of the title compound exhibits higher

Table 9

Result of the title compound 2C2Os molecular docking with several Anemia proteins 7KPI, 5MWP, 4NJ8, and 6RTX.

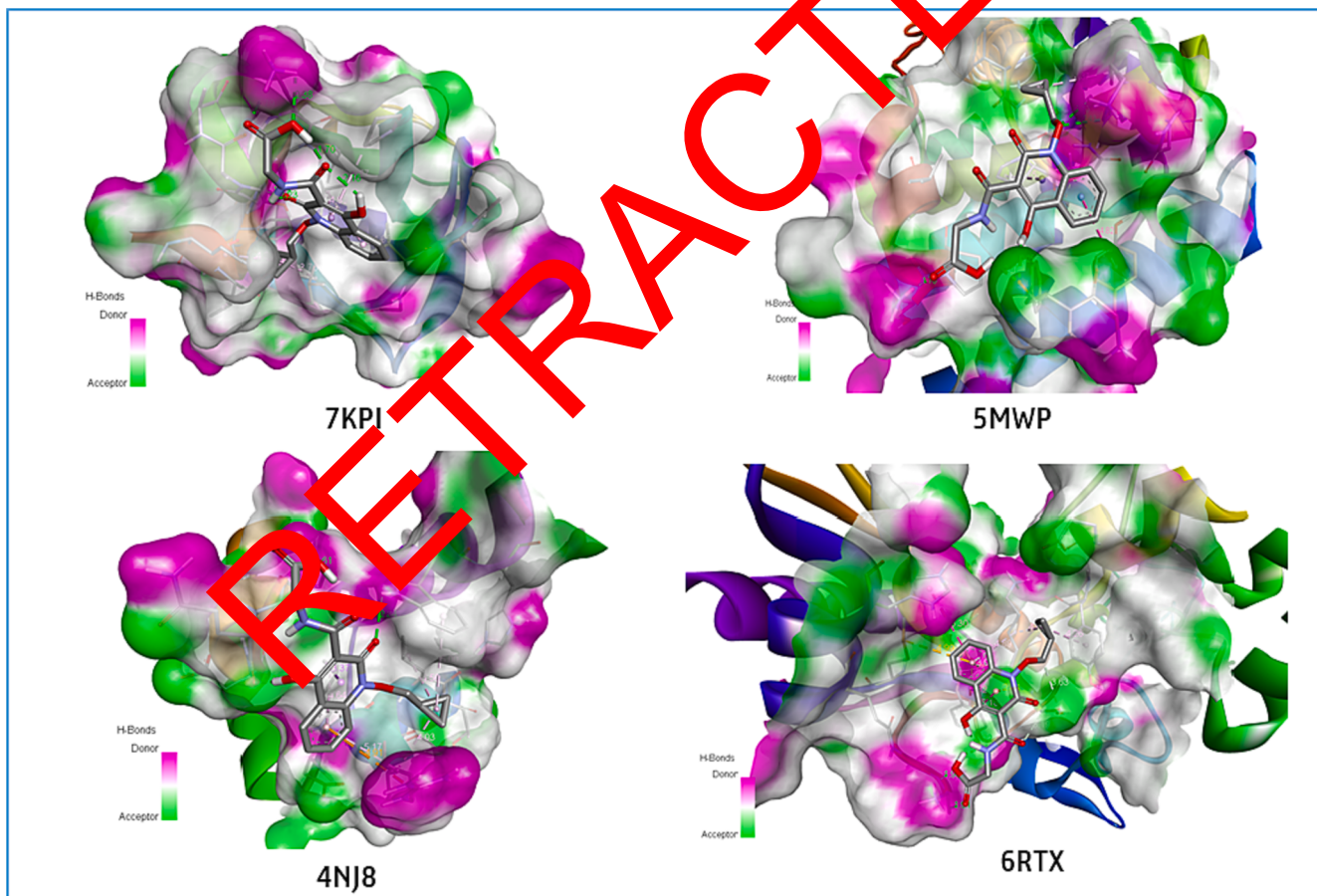
Protein (PDB CODE)	Type of organism	Binding affinity (kcal/mol)	Inhibition constant (μM)	Inter molecular energy (kcal/mol)	Electrostatic energy (kcal/mol)	Reference RMSD (Å)	Bonded Residues
7KPI	Homo sapiens	-7.08	6.51	-9.46	-2.34	12.61	ALA61, LYS64, VAL30, VAL163, LEU65, LYS28, PRO94, VAL98
5MWP	Homo sapiens	-6.39	20.62	-8.78	-1.76	17.05	PHE732, LYS791, SER737, TYR731, PRO788
4NJ8	Homo sapiens	-5.52	90.33	-7.9	-1.56	21.08	TRP66, PRO8, GLN9, LEU34, LEU38, ARG35
6RTX	Homo sapiens	-5.26	139.76	-7.65	-1.76	35.71	ALA151, TYR204, HIS375, TYR2245, LYS205, SER206

Table 10

The ligand 2C2Os Non – Covalent interactions with the Anemia disease proteins 7KPI,5MWP,4NJ8 & 6RTX.

Protein	Binding Energy (kcal/mol)	Ligand groups	Protein Residues	*Type of interaction	Distance (Å)	Protein	Binding Energy (kcal/mol)	Ligand groups	Protein Residues	*Type of interaction	Distance (Å)
7KPI	-7.08	CO	ALA61	COHB	1.79	4NJ8	-5.52	CO	TRP66	COHB	2.84
		CO	LYS64	COHB	1.79			CO	PRO8	COHB	1.61
		CO	LYS64	COHB	2.39			NH	PRO8	COHB	2.2
		CH	LEU65	AL	5.15			OH	GLN9	COHB	2.21
		CH _{ring}	LEU65	PAL	4.29			CH _{ring}	LEU34	PS	4.64
		CH _{ring}	LEU65	PAL	5.26			CH	LEU38	AL	4.5
		CH	VAL30	AL	4.9			CH	ARG35	PCN	4.91
		CH	VAL163	AL	3.76			CO	ALA151	COHB	1.91
		CH _{ring}	LYS28	AL	4.32			CO	ALA51	COHB	1.96
		CH _{ring}	PRO94	PAL	4.85			OH	TYR204	COHB	2.06
		CH _{ring}	VAL98	PAL	4.77			OH	TYR204	COHB	2.22
		OH	PHE732	COHB	2.25			CH _{ring}	TYR204	PPTS	5.16
		OH	PHE732	COHB	2.47			CH _{ring}	TYR204	PPTS	5.32
5MWP	-6.39	CO	SER737	COHB	1.7			CH _{ring}	HIS375	PPS	5.3
		CH _{ring}	TYR731	PPTS	4.82			CH	TYR224	PAL	4.26
		CH _{ring}	PRO788	PAL	4.65			CH	LYS25	PDHB	3.05
								CO	SER200	CHB	3.19
								CO	SER206	CHB	3.63

* COHB-CONVENTIONAL HYDROGEN BOND, PAL-π-Alkyl, PPTS - π - π T-shaped, AL-Alkyl, PCN - π-Cation, PPS - π-π STACKING, PDHB - π-DONOR HYDROGEN BOND, CHB - Carbon Hydrogen Bond, PS - π-SIGMA.

**Fig. 9a.** 3D Molecular docking of compound 2C2O with Anemia of Chronic kidney disease proteins.

stability for the chosen proteins.

CRediT authorship contribution statement

P. Manikandan: Validation, Visualization, Writing – original draft, Writing – review & editing. **M. Kumar:** Supervision, Validation,

Visualization, Resources, Methodology, Project administration. **S. Chithra:** Validation, Visualization, Resources, Conceptualization, Data curation, Formal analysis, Investigation. **A. Jeelani:** Validation, Visualization, Resources, Conceptualization, Data curation. **Jamal M. Khaled:** Data curation, Formal analysis, Funding acquisition, Investigation, Software. **Ghulam Abbas:** Formal analysis, Funding acquisition,

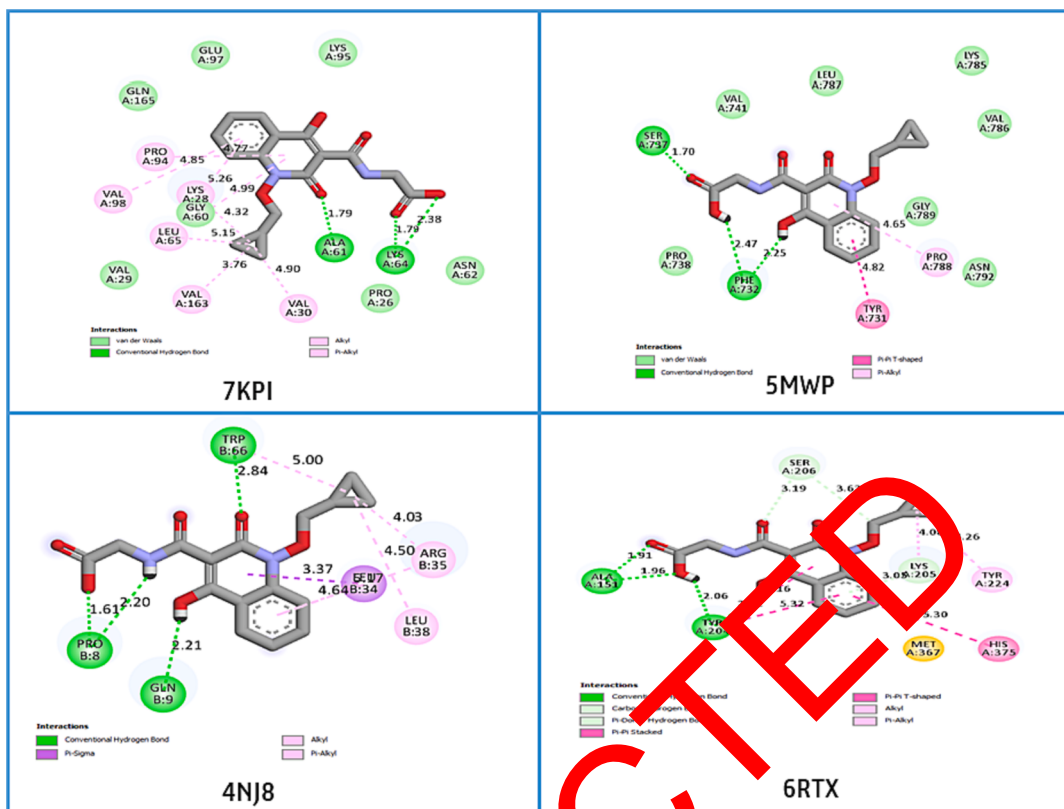


Fig. 9b. 2D molecular docking images of 2C2O compound with Anemia of Chronic kidney disease proteins.

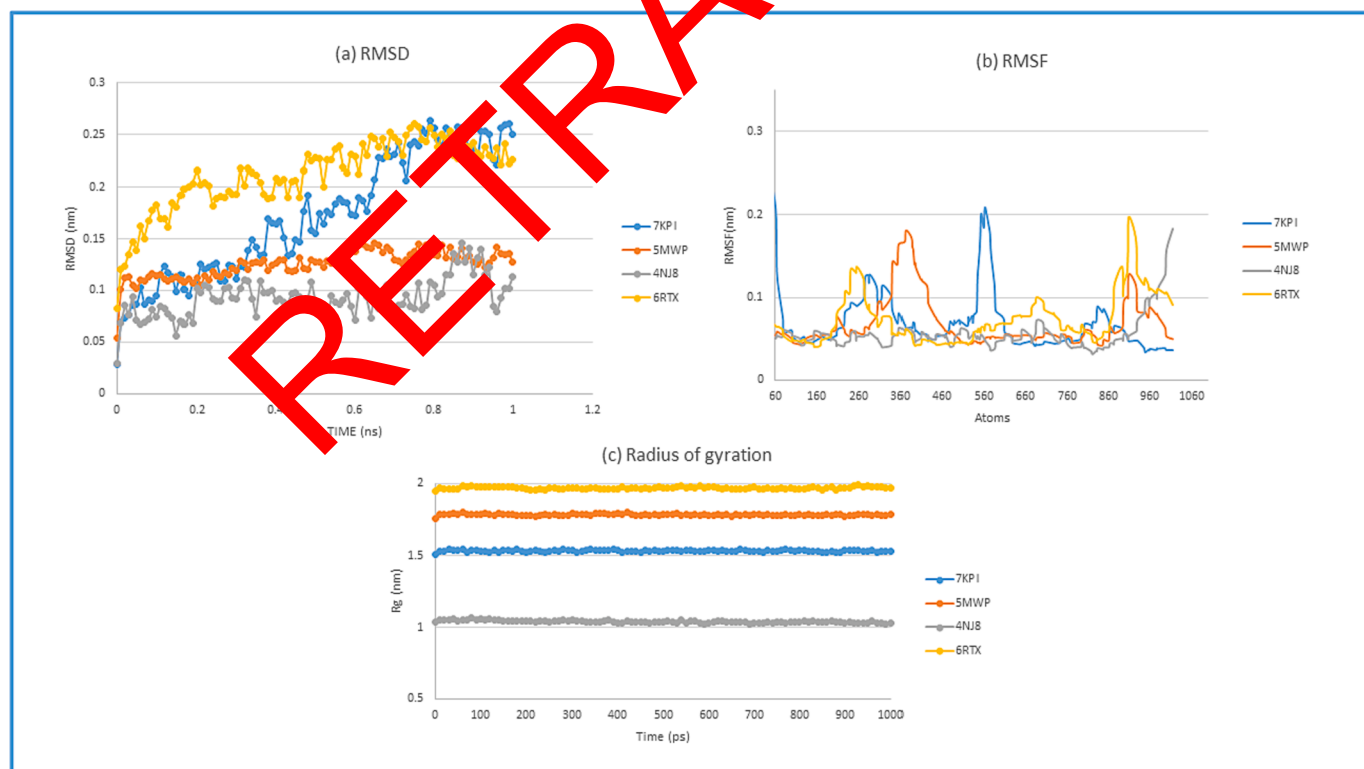


Fig. 10. (a) RMSD studies of Protein-ligand targets (b) RMSF studies of Protein-ligand targets (c) Radius of gyration (R_g) studies of Protein-ligand targets.

Investigation, Software. **S. Muthu:** Supervision, Validation, Visualization, Resources, Conceptualization, Data curation, Formal analysis, Funding acquisition, Investigation.

Declaration of Competing Interest

The authors declare that they have no known competing financial interests or personal relationships that could have appeared to influence the work reported in this paper.

Data availability

Data will be made available on request.

Acknowledgement

The authors extend their appreciation to the Deputyship for Research and Innovation, "Ministry of Education" in Saudi Arabia for funding this research (IFKSUOR3-457-1).

References

- [1] B. Alcaide, P. Almendros, C. Aragoncillo, ChemInform abstract: highly reactive 4-membered ring nitrogen-containing heterocycles: synthesis and properties, *ChemInform* 42 (20) (2011) 685–697, <https://doi.org/10.1002/chin.201120235>.
- [2] F. Gao, X. Zhang, T. Wang, J. Xiao, Quinolone hybrids and their anti-cancer activities: an overview, *Eur. J. Med. Chem.* 165 (2019) 59–79, <https://doi.org/10.1016/j.ejmech.2019.01.017>.
- [3] E.A.E. El-Helw, A.I. Hashem, Synthesis and antitumor activity evaluation of some pyrrolone and pyridazinone heterocycles derived from 3-((2-oxo-5-(p-tolyl)furan-3(2H)-ylidene)methyl)quinolin-2(1H)-one, *Synth. Commun.* 50 (7) (2020) 1046–1055, <https://doi.org/10.1080/00397911.2020.1731549>.
- [4] E.A.E. El-Helw, A.R.I. Morsy, A.I. Hashem, Evaluation of some new heterocycles bearing 2-oxoquinolyl moiety as immunomodulator against highly pathogenic avian influenza virus (H5 N 8), *J. Heterocycl. Chem.* 58 (4) (2021) 1003–1011, <https://doi.org/10.1002/jhet.4233>.
- [5] F. Gao, P. Wang, H. Yang, Q. Miao, L. Ma, G. Lu, Recent developments of quinolone-based derivatives and their activities against *Escherichia coli*, *Eur. J. Med. Chem.* 157 (2018) 1223–1248, <https://doi.org/10.1016/j.ejmech.2018.08.095>.
- [6] J.H. Xu, Y.L. Fan, J. Zhou, Quinolone-triazole hybrids and their biological activities, *J. Heterocycl. Chem.* 55 (8) (2018) 1854–1862, <https://doi.org/10.1002/jhet.3234>.
- [7] A. El-Gazzar, H. Hafez, G. Nawwar, New acyclic nucleosides analogues as potential analgesic, anti-inflammatory, anti-oxidant and anti-microbial agents derived from pyrimido[4,5-b]quinolines, *Eur. J. Med. Chem.* 44 (4) (2009) 1427–1436, <https://doi.org/10.1016/j.ejmech.2008.09.030>.
- [8] E.A.E. El-Helw, A.A. El-Badawy, Synthesis of chromanone, pyrimidinone, thiazoline and quinolone derivatives as prospective antitumor agents, *J. Heterocycl. Chem.* 57 (6) (2020) 2354–2364, <https://doi.org/10.1002/jhet.3948>.
- [9] A.H. Kategaonkar, R.U. Pokalwar, S. Sonary, U. Ganapati, B.B. Shingate, M. S. Shingare, Synthesis, in vitro antibacterial and antifungal evaluations of new α -hydroxyphosphonate and new α -acetoxyphosphonate derivatives of tetrazolo [1, 5-a] quinolone, *Eur. J. Med. Chem.* 53 (Suppl. 1) (2012) 1128–1132, <https://doi.org/10.1016/j.ejmech.2009.12.013>.
- [10] A.M. El-Naggar, S.K. Ramadan, Efficient synthesis of some pyrimidine and thiazolidine derivatives bearing quinoline scaffold under microwave irradiation, *Synth. Commun.* 50 (14) (2020) 2188–2198, <https://doi.org/10.1080/00397911.2020.1769673>.
- [11] P. Palit, P. Paira, A. Hazra, S. Banerjee, A.D. Gupta, S.G. Dastidar, N.B. Mondal, Phase transfer catalyzed synthesis of bis-quinolines: antileishmanial activity in experimental visceral leishmaniasis and in vitro antibacterial evaluation, *Eur. J. Med. Chem.* 44 (2) (2009) 845–853, <https://doi.org/10.1016/j.ejmech.2008.04.014>.
- [12] X.D. Jia, S. Wang, M.H. Wang, M.L. Liu, G.M. Xia, X.J. Liu, Y. Chai, H.W. He, Synthesis and in vitro antitumor activity of novel naphthyridinone derivatives, *Chin. Chem. Lett.* 28 (2) (2017) 235–239, <https://doi.org/10.1016/j.ccl.2016.07.024>.
- [13] K.C. Sekgota, S. Majumder, M. Isaacs, D. Mnkanhla, H.C. Hoppe, S.D. Khanye, F. H. Kriel, J. Coates, P.T. Kaye, Application of the Morita-Baylis-Hillman reaction in the synthesis of 3-[(N -cycloalkylbenzamido)methyl]-2-quinolones as potential HIV-1 integrase inhibitors, *Bioorg. Chem.* 75 (2017) 310–316, <https://doi.org/10.1016/j.bioorg.2017.09.015>.
- [14] N.M. Gad, W.S.I. Abou-Elmagd, D.S.A. Haneen, S.K. Ramadan, Reactivity of 5-phenyl-3-[(2-chloroquinolin-3-yl)methylene] furan-(3H)-one towards hydrazine and benzylamine: a comparative study, *Synth. Commun.* 51 (9) (2021) 1384–1397, <https://doi.org/10.1080/00397911.2021.1882498>.
- [15] P.C. Sharma, A. Jain, S. Jain, Fluoroquinolone antibacterials: a review on chemistry, microbiology and therapeutic prospects, *Acta Pol. Pharm.* 66 (6) (2009) 587–604.
- [16] J.V. Jun, E.J. Petersson, D.M. Chenoweth, Rational design and facile synthesis of a highly tunable quinoline-based fluorescent small-molecule scaffold for live cell imaging, *J. Am. Chem. Soc.* 140 (30) (2018) 9486–9493, <https://doi.org/10.1021/jacs.8b03738>.
- [17] S. Dhillon, Desudostat: first approval, *Drugs* 82 (11) (2022) 1207–1212, <https://doi.org/10.1007/s40265-022-01744-w>.
- [18] M.J. Frisch, G.W. Trucks, H.B. Schlegel, G.E. Scuseria, M.A. Robb, J.R. Cheeseman, Gaussian 09, C3 Revision B. 01, Gaussian Inc., Wallingford CT, 2010.
- [19] M.H. Jamróz, Vibrational energy distribution analysis (VEDA): scopes and limitations, *Spectrochim. Acta Part A: Mol. Biomol. Spectrosc.* 114 (2013) 220–230, <https://doi.org/10.1016/j.saa.2013.05.096>.
- [20] T. Lu, F. Chen, Multiwfn: a multifunctional wavefunction analyzer, *J. Comput. Chem.* 33 (5) (2011) 580–592, <https://doi.org/10.1002/jcc.22885>.
- [21] G.M. Morris, R. Huey, W. Lindstrom, M.F. Sanner, R.K. Belew, D.S. Goodsell, A. J. Olson, AutoDock4 and AutoDockTools4: automated docking with selective receptor flexibility, *J. Comput. Chem.* 30 (16) (2009) 2785–2791, <https://doi.org/10.1002/jcc.21256>.
- [22] G.A. Andrienko, Chemcraft-graphical software for visualization of quantum chemistry computations, 2010, See <https://www.chemcraftprog.com>.
- [23] E. Eunice, J.C. Prasana, S. Muthu, A. Muradha, Molecular structure, spectroscopic, quantum computational, and molecular docking investigations on propyl gallate, *Polycycl. Aromat. Compd.* 42 (2022) 1–21, <https://doi.org/10.1080/10406638.2022.2107688>.
- [24] E.B. Wilson J.C. Decius, C.C. Cross, *Molecular Vibrations: The Theory of Infrared and Raman Vibrational Spectra*, 2012.
- [25] Silverstein, G.C. Bassler, T.C. Morrill, *Infrared identification of organic compounds* (Fifth Edition), R. M. Wiley, New York, 1991.
- [26] A.K. Srivastava, B. Prayana, B.K. Barojini, N. Misra, Vibrational, structural and hydrogen bonding analysis of N-(E)-4-Hydroxybenzylidene]-2-(naphthalen-2-yloxy)-3-hydrazide: calculated density functional and atoms-in-molecule based theoretical studies, *Indian J. Phys.* 88 (6) (2014) 547–556, <https://doi.org/10.1007/s12648-014-0449-y>.
- [27] S. Muthu, G. Ma, M. Kumar, S. Muthu, A. Saraf, F.B. Asif, A. Irfan, Antimicrobial activity, molecular profiling, electronic properties and molecular docking investigation of 5-[1-hydroxy-2-(isopropylamino)ethyl]benzene-3-diol, *J. Mol. Struct.* 1247 (2022), 131299, <https://doi.org/10.1016/j.molstruc.2021.131299>.
- [28] S. Elling, D. Williams, *Spectroscopic Methods in Organic Chemistry*, 2019, doi: 10.1007/978-3-030-18252-6.
- [29] K. Bhavani, S. Renuga, S. Muthu, K. Sankara Narayanan, Quantum mechanical study and spectroscopic (FT-IR, FT-Raman, 13C, 1H) study, first order hyperpolarizability, NBO analysis, HOMO and LUMO analysis of 2-acetoxybenzoic acid by density functional methods, *Spectrochim Acta Part A: Mol. Biomol. Spectrosc.* 136 (2015) 1260–1268, <https://doi.org/10.1016/j.saa.2014.10.012>.
- [30] A. Choperena, P. Painter, An infrared spectroscopic study of hydrogen bonding in ethyl phenol: a model system for polymer phenolics, *Vib. Spectrosc.* 51 (1) (2009) 110–118, <https://doi.org/10.1016/j.vibspec.2008.11.008>.
- [31] L.J. Bellamy, The infra-red spectra of complex molecules (1975), <https://doi.org/10.1007/978-94-011-6017-9>.
- [32] S. Gunasekaran, E. Sailatha, S. Srinivasan, S. Kumaresan, FTIR, FT Raman spectra and molecular structural confirmation of isoniazid, *Indian J. Pure Appl. Phys.* 47 (2009) 12–18.
- [33] V. Krishnakumar, R.J. Xavier, Normal coordinate analysis of 2-mercapto and 4,6-dihydroxy-2-mercapto pyrimidines, *Indian J. Pure Appl. Phys.* 41 (2003) 597–601.
- [34] S. Seshadri, S. Gunasekaran, S. Muthu, S. Kumaresan, R. Arunbalaji, Vibrational spectroscopy investigation using ab initio and density functional theory on flucytosine, *J. Raman Spectrosc.* 38 (11) (2007) 1523–1531, <https://doi.org/10.1002/jrs.1808>.
- [35] H. Tanak, F. Ersahin, E. Agar, O. Büyükgüngör, M. Yavuz, Crystal structure of n-2-methoxyphenyl-2-oxo-5-nitro-1-benzylidene-methylamine, *Anal. Sci.* 24 (2008) 237–238, <https://doi.org/10.1116/analscix.24.x237>.
- [36] N. Sundaraganesan, S. Illakiamani, C. Meganathan, B.D. Joshua, Vibrational spectroscopy investigation using ab initio and density functional theory analysis on the structure of 3-aminobenzotri fluoride, *Spectrochim. Acta Part A: Mol. Biomol. Spectrosc.* 67 (1) (2007) 214–224, <https://doi.org/10.1016/j.saa.2006.07.004>.
- [37] M. Karabacak, M. Cinar, M. Kurt, A. Poiyamozihi, N. Sundaraganesan, The spectroscopic (FT-IR, FT-Raman, UV and NMR) first order hyperpolarizability and HOMO-LUMO analysis of dansyl chloride, *Spectrochim. Acta Part A: Mol. Biomol. Spectrosc.* 117 (2014) 234–244, <https://doi.org/10.1016/j.saa.2013.07.095>.
- [38] M. Karabacak, M. Kurt, M. Çınar, A. Çoruh, Experimental (UV, NMR, IR and Raman) and theoretical spectroscopic properties of 2-chloro-6-methylaniline, *Mol. Phys.* 107 (3) (2009) 253–264, <https://doi.org/10.1080/0026897090281579>.
- [39] C.S. Abraham, J.C. Prasana, S. Muthu, B. Rizwana, M. Raja, Quantum computational studies, spectroscopic (FT-IR, FT-Raman and UV-Vis) profiling, natural hybrid orbital and molecular docking analysis on 2,4-Dibromoaniline, *J. Mol. Struct.* 1160 (2018) 393–405, <https://doi.org/10.1016/j.molstruc.2018.02.022>.
- [40] P. Fuentealba, E. Chamorro, J.C. Santos, Chapter 5 Understanding and using the electron localization function, *Theor. Comput. Chem.* (2007) 57–85, doi: 10.1016/s1380-7323(07)80006-9.
- [41] P. Politzer, P.R. Laurence, K. Jayasuriya, Molecular electrostatic potentials: an effective tool for the elucidation of biochemical phenomena, *Environ. Health Perspect.* 61 (1985) 191–202, <https://doi.org/10.1289/ehp.8561191>.

- [42] M. Raja, R. Raj Muhamed, S. Muthu, M. Suresh, Synthesis, spectroscopic (FT-IR, FT-Raman, NMR, UV-Visible), NLO, NBO, HOMO-LUMO, Fukui function and molecular docking study of (E)-1-(5-bromo-2-hydroxybenzylidene)semicarbazide, *J. Mol. Struct.* 1141 (2017) 284–298, <https://doi.org/10.1016/j.molstruc.2017.03.117>.
- [43] S. Sevvanthi, S. Muthu, M. Raja, Quantum mechanical, spectroscopic studies and molecular docking analysis on 5,5-diphenylimidazolidine-2,4-dione, *J. Mol. Struct.* 1149 (2017) 487–498, <https://doi.org/10.1016/j.molstruc.2017.08.015>.
- [44] P. Thul, V. Gupta, V. Ram, P. Tandon, Structural and spectroscopic studies on 2-pyranones, *Spectrochim. Acta Part A: Mol. Biomol. Spectrosc.* 75 (1) (2010) 251–260, <https://doi.org/10.1016/j.saa.2009.10.020>.
- [45] V. Choudhary, A. Bhatt, D. Dash, N. Sharma, DFT calculations on molecular structures, HOMO-LUMO study, reactivity descriptors and spectral analyses of newly synthesized diorganotin(IV) 2-chloridophenylacetohydroxamate complexes, *J. Comput. Chem.* 40 (27) (2019) 2354–2363, <https://doi.org/10.1002/jcc.26012>.
- [46] O. El-Gammal, G. Abu El-Reash, S. Ghazy, A. Radwan, Synthesis, characterization, molecular modeling and antioxidant activity of (1E,5E)-1,5-bis(1-(pyridin-2-yl) ethylidene)carbonohydrazide (H2APC) and its zinc(II), cadmium(II) and mercury (II) complexes, *J. Mol. Struct.* 1020 (2012) 6–15, <https://doi.org/10.1016/j.molstruc.2012.04.029>.
- [47] G. Abu El-Reash, O. El-Gammal, A. Radwan, Molecular structure and biological studies on Cr(III), Mn(II) and Fe(III) complexes of heterocyclic carbohydrazone ligand, *Spectrochim. Acta Part A: Mol. Biomol. Spectrosc.* 121 (2014) 259–267, <https://doi.org/10.1016/j.saa.2013.10.048>.
- [48] A. Jelani, S. Muthu, B.R. Rajaraman, S. Sevvanthi, Spectroscopic, quantum chemical calculations, and molecular docking analysis of 3-Chlorophenyl boronic acid, *Spectrosc. Lett.* 53 (10) (2020) 778–792, <https://doi.org/10.1080/00387010.2020.1834410>.
- [49] E.R. Johnson, S. Keinan, P. Mori-Sánchez, J. Contreras-García, A.J. Cohen, W. Yang, Revealing noncovalent interactions, *J. Am. Chem. Soc.* 132 (18) (2010) 6498–6506, <https://doi.org/10.1021/ja100936w>.
- [50] S.S. Khemalapure, V.S. Katti, C.S. Hiremath, S.M. Hiremath, M. Basanagouda, S. B. Radher, Spectroscopic (FT-IR, FT-Raman, NMR and UV-Vis), ELF, LOL, NBO, and Fukui function investigations on (5-bromo-benzofuran-3-yl)-acetic acid hydrazide (5BBAH): experimental and theoretical approach, *J. Mol. Struct.* 1196 (2019) 280–290, <https://doi.org/10.1016/j.molstruc.2019.06.078>.
- [51] S. Cherian Parakkal, R. Datta, A. Saral, S. Muthu, A. Irfan, A. Jelani, Solvent polarity, structural and electronic properties with different solvents and biological studies of 3,3,5-triphenylfuran-2(3H)-one- cancers of the blood cells, *J. Mol. Liq.* 368 (2022), 120674, <https://doi.org/10.1016/j.jmoliq.2022.120674>.
- [52] M. Govindarajan, M. Karabacak, S. Periandy, D. Tanuja, Spectroscopic (FT-IR, FT-Raman, UV and NMR) investigation and NLO, HOMO-LUMO, NBO analysis of organic 2,4,5-trichloroaniline, *Spectrochim. Acta Part A: Mol. Biomol. Spectrosc.* 97 (2012) 231–245, <https://doi.org/10.1016/j.saa.2012.06.014>.
- [53] R. Vijayaraj, V. Subramanian, P.K. Chattaraj, Comparison of global capacity descriptors calculated using various density functionals: a QSAR perspective, *J. Chem. Theory Comput.* 5 (10) (2009) 2744–2753, <https://doi.org/10.1021/ct900347f>.
- [54] F. Weinhold, C.R. Landis, Natural bond orbitals and extensions of localized bonding concepts, *Chem. Educ. Res. Pract.* 2 (2) (2001) 91–104, <https://doi.org/10.1039/B1rp90011k>.
- [55] R. Behjatmanesh-Ardakani, M. Arab, A. Saleem, Z. Mosapour, S. Bin Mohamad, NBO-NEDA and AIM Studies on the Interactions between Benzocryptand [222B] and Li⁺, Na⁺, K⁺ and Ca²⁺, *Int. J. Pharm. Sci. Rev. Res.* 39 (2016) 45–53.
- [56] J. Choo, S. Kim, H. Joo, Y. Kwon, Molecular structures of (trifluoromethyl)iodine dihalides CF3IX2 (X=F, Cl): ab initio and DFT calculations, *J. Mol. Struct. (Theochem.)* 587 (1–3) (2002) 1–8, [https://doi.org/10.1016/s0166-1280\(02\)00107-0](https://doi.org/10.1016/s0166-1280(02)00107-0).
- [57] P. Govindasamy, S. Gunasaran, C. Selvamalar, Natural bond orbital analysis, electronic structure and vibrational spectral analysis of N-(4-hydroxy phenyl) acetamide: a density functional theory, *Spectrochim. Acta Part A: Mol. Biomol. Spectrosc.* 130 (2014) 621–633, <https://doi.org/10.1016/j.saa.2014.03.065>.
- [58] J.P. Foster, F. Weinhold, Natural hybrid orbitals, *J. Am. Chem. Soc.* 102 (24) (1980) 7211–7218, <https://doi.org/10.1021/ja00544a007>.
- [59] A.E. Reed, R.B. Weinstein, F. Weinhold, Natural population analysis, *J. Chem. Phys.* 83 (2) (1985) 735–746, <https://doi.org/10.1063/1.449486>.
- [60] B.K. Paul, S. Mahanta, R.B. Singh, N. Guchhait, A DFT-based theoretical study on the photophysics of 4-hydroxyacridine: single-water-mediated excited state proton transfer, *J. Phys. Chem. A* 114 (7) (2010) 2618–2627, <https://doi.org/10.1021/jp909029c>.
- [61] L. Li, C. Wu, Z. Wang, L. Zhao, Z. Li, C. Sun, T. Sun, Density functional theory (DFT) and natural bond orbital (NBO) study of vibrational spectra and intramolecular hydrogen bond interaction of L-ornithine-L-aspartate, *Spectrochim. Acta Part A: Mol. Biomol. Spectrosc.* 136 (2015) 338–346, <https://doi.org/10.1016/j.saa.2014.08.153>.
- [62] R.S. Mulliken, Electronic population analysis on LCAO–MO molecular wave functions. I, *J. Chem. Phys.* 23 (10) (1955) 1833–1840, <https://doi.org/10.1063/1.1740588>.
- [63] P.W. Ayers, R.G. Parr, Variational principles for describing chemical reactions: the Fukui function and chemical hardness revisited, *J. Am. Chem. Soc.* 122 (9) (2000) 2010–2018, <https://doi.org/10.1021/ja9924039>.
- [64] W. Yang, W.J. Mortier, The use of global and local molecular parameters for the analysis of the gas-phase basicity of amines, *J. Am. Chem. Soc.* 108 (19) (1986) 5708–5711, <https://doi.org/10.1021/ja00279a008>.
- [65] W. Yang, R.G. Parr, Hardness, softness, and the Fukui function in the electronic theory of metals and catalysis, *Proc. Natl. Acad. Sci.* 82 (20) (1985) 6723–6726, <https://doi.org/10.1073/pnas.82.20.6723>.
- [66] T.K. Kuruvilla, J.C. Prasana, S. Muthu, J. George, Vibrational spectroscopic (FT-IR, FT-Raman) and quantum mechanical study of 4-(2-chlorophenyl)-2-ethyl-9-methyl-6H-thieno[3,2-f][1,2,4]triazolo[4-a][1,4] diazepine, *J. Mol. Struct.* 1157 (2018) 519–529, <https://doi.org/10.1016/j.molstruc.2018.01.001>.
- [67] K. Fukui, Role of Frontier orbitals in chemical reactions, *Science* 218 (4574) (1982) 747–754, <https://doi.org/10.1126/science.218.4574.747>.
- [68] A. Klamt, C. Moya, J. Palomar, A comprehensive comparison of the IEFPCM and SS (V)PE continuum solvation methods with the COSMO approach, *J. Chem. Theory Comput.* 11 (9) (2015) 4220–4225, <https://doi.org/10.1021/acs.jctc.5b00601>.
- [69] A. Esme, S. Sagdic, Conformational, spectroscopic (FT-IR, FT-Raman, and UV-Vis), and molecular docking studies of N-(2-hydroxyethyl) succinimide, *J. Mol. Struct.* 1195 (2019) 451–461, <https://doi.org/10.1016/j.molstruc.2019.06.019>.
- [70] S. Trabelsi, N. Issaoui, S.A. Brandán, F. Bardak, T. Roisnel, A. Atac, H. Marouani, Synthesis and physico-chemical properties of a novel chromatic compound with potential biological applications, bis(2-phenylethylammonium) chromate(VI), *J. Mol. Struct.* 1185 (2019) 168–182, <https://doi.org/10.1016/j.molstruc.2019.02.106>.
- [71] H. Jacobsen, Hypovalency—a kinetic-energy density description of a 4c–2e bond, *Dalton Trans.* 21 (2009) 4252, <https://doi.org/10.1039/b823382a>.
- [72] R.S. Saji, J.C. Prasana, S. Muthu, J. George, T.K. Kuruvilla, B. Raajaraman, Spectroscopic and quantum computation study on naproxen sodium, *Spectrochim. Acta Part A: Mol. Biomol. Spectrosc.* 226 (2020), 117614, <https://doi.org/10.1016/j.saa.2019.117614>.
- [73] B. Riwana, S. Muthu, J.C. Prasana, C.S. Abraham, M. Raja, Spectroscopic (FT-IR, FT-Raman) investigation topology (CSP, FCF, LOL) analyses, charge transfer excitation and molecular docking (desolv, HCV) studies on ribavirin, *Chem. Data Collect.* 17–18 (2018) 229–250, <https://doi.org/10.1016/j.cdc.2018.09.003>.
- [74] J. Contreras-García, M. Boto, F. Alquero-Ruiz, I. Reva, T. Woller, M. Alonso, A benchmark for the non-covalent interaction (NCI) index or ... is it really all in the geometry? *Theor. Chem. Acc.* 135(10) (2016), doi: 10.1007/s00214-016-1977-7.
- [75] B. Riwana, S. Muthu, J.C. Prasana, C.S. Abraham, S. Muthu, Spectroscopic investigation, NBO, surface analysis and molecular docking studies on anti-HIV drug entecavir, *J. Mol. Struct.* 1164 (2018) 447–458, <https://doi.org/10.1016/j.molstruc.2018.03.090>.
- [76] G.Y. Li, J. Geng, C.H. He, G.H. Cui, Structure, spectroscopy, and theory calculation on 1,3-bis((5,6-dimethyl-1H-benzod[d]imidazol-1-yl)methyl)benzene, *J. Mol. Struct.* 1031 (2013) 56–60, <https://doi.org/10.1016/j.jPCA.2012.07.014>.
- [77] J.R. Proudfoot, Drugs, leads, and drug-likeness: an analysis of some recently launched drugs, *Bioorg. Med. Chem. Lett.* 12 (12) (2002) 1647–1650, [https://doi.org/10.1016/s0960-894x\(02\)00244-5](https://doi.org/10.1016/s0960-894x(02)00244-5).
- [78] J. Mazumder, R. Chakraborty, S. Sena, S. Vadrab, B. Dec, T.K. Ravi, Synthesis and biological evaluation of some novel quinoxalinyl triazole derivatives, *Der Pharma Chem* 1 (2009) 188–198.
- [79] G. Vistoli, A. Pedretti, B. Testa, Assessing drug-likeness – what are we missing? *Drug Discov. Today* 13 (7–8) (2008) 285–294, <https://doi.org/10.1016/j.drudis.2007.11.007>.
- [80] D.F. Veber, S.R. Johnson, H.Y. Cheng, B.R. Smith, K.W. Ward, K.D. Kopple, Molecular properties that influence the oral bioavailability of drug candidates, *J. Med. Chem.* 45 (12) (2002) 2615–2623, <https://doi.org/10.1021/jm02017n>.
- [81] C.A. Lipinski, F. Lombardo, B.W. Dominy, P.J. Feeney, Experimental and computational approaches to estimate solubility and permeability in drug discovery and development settings, *Adv. Drug Del. Rev.* 23 (1–3) (1997) 3–25, [https://doi.org/10.1016/s0169-409x\(96\)00423-1](https://doi.org/10.1016/s0169-409x(96)00423-1).
- [82] A.L. Hopkins, G.M. Keserü, P.D. Leeson, D.C. Rees, C.H. Reynolds, The role of ligand efficiency metrics in drug discovery, *Nat. Rev. Drug Discov.* 13 (2) (2014) 105–121, <https://doi.org/10.1038/nrd4163>.
- [83] P.D. Leeson, B. Springthorpe, The influence of drug-like concepts on decision-making in medicinal chemistry, *Nat. Rev. Drug Discov.* 6(11) (2007) 881–890, doi: 10.1038/nrd2445.
- [84] A. Daina, O. Michielin, V. Zoete, SwissADME: a free web tool to evaluate pharmacokinetics, drug-likeness and medicinal chemistry friendliness of small molecules - Scientific Reports, *Nature* (2017), doi: 10.1038/srep42717.
- [85] X.Y. Meng, H.X. Zhang, M. Mezei, M. Cui, Molecular docking: a powerful approach for structure-based drug discovery, *Curr. Comput. Aided-Drug Des.* 7 (2) (2011) 146–157, <https://doi.org/10.2174/157340911795677602>.
- [86] H. Li, H.Y. Wang, S. Kang, R.B. Silverman, T.L. Poulos, Electrostatic control of isoform selective inhibitor binding in nitric oxide synthase, *Biochemistry* 55 (26) (2016) 3702–3707, <https://doi.org/10.1021/acs.biochem.6b00261>.
- [87] M. Vraneš, S. Armaković, A. Tot, S. Papović, N. Zec, S. Armaković, N. Banić, B. Abramović, S. Gadžurić, Structuring of water in the new generation ionic liquid – comparative experimental and theoretical study, *J. Chem. Thermodyn.* 93 (2016) 164–171, <https://doi.org/10.1016/j.jct.2015.10.001>.
- [88] S. Armaković, S.J. Armaković, S. Pelešić, D. Mirjanić, Influence of sumanene modifications with boron and nitrogen atoms to its hydrogen adsorption properties, *PCCP* 18 (4) (2016) 2859–2870, <https://doi.org/10.1039/c5cp04497a>.
- [89] M.J. Abraham, T. Murtola, R. Schulz, S. Páll, J.C. Smith, B. Hess, E. Lindahl, GROMACS: High performance molecular simulations through multi-level parallelism from laptops to supercomputers, *SoftwareX* 1–2 (2015) 19–25, <https://doi.org/10.1016/j.softx.2015.06.001>.
- [90] V. Zoete, M.A. Cuendet, A. Grosdidier, O. Michielin, SwissParam: a fast force field generation tool for small organic molecules, *J. Comput. Chem.* 32 (11) (2011) 2359–2368, <https://doi.org/10.1002/jcc.21816>.

- [91] K. Jacob, S. Ganguly, P. Kumar, R. Poddar, A. Kumar, Homology model, molecular dynamics simulation and novel pyrazole analogs design of *Candida albicans* CYP450 lanosterol 14 α -demethylase, a target enzyme for antifungal therapy, J. Biomol. Struct. Dyn. 35 (7) (2016) 1446–1463, <https://doi.org/10.1080/07391102.2016.1185380>.
- [92] B. Pandey, P. Sharma, Structural insights into impact of Y134F mutation and discovery of novel fungicidal compounds against CYP51 in *Puccinia triticina*, J. Cell. Biochem. 119 (3) (2017) 2588–2603, <https://doi.org/10.1002/jcb.26422>.
- [93] V. Jeba Reeda, P. Divya, R. Suja, A. Rathika, V. Bena Jothy, Synthesis, spectroscopic investigations, topological non-covalent interactions, chemical reactivity, molecular docking and molecular dynamic simulation on piperazine succinate - a potential antimicrobial compound, J. Mol. Struct. 1292 (2023), 136179, <https://doi.org/10.1016/j.molstruc.2023.136179>.

RETRACTED